D. BORISYUK,[1] A. KOBUSHKIN[1, 2]

[1] Bogolyubov Institute for Theoretical Physics, Nat. Acad. of Sci. of Ukraine
(14b, Metrolohichna Str., Kyiv 03143, Ukraine)
[2] National Technical University of Ukraine "Igor Sikorsky KPI"
(37, Peremogy Prosp., Kyiv 03056, Ukraine)

UDC 539

TWO-PHOTON EXCHANGE IN ELASTIC ELECTRON SCATTERING ON HADRONIC SYSTEMS

In the present review, we discuss different aspects of the two-photon exchange (TPE) physics in elastic ep scattering at high Q^2, as well as at low Q^2. The imaginary part of the TPE amplitude gives rise to beam and target single-spin asymmetries. Different theoretical approaches to the calculation of these observables are considered. The real part of the TPE amplitude influences the unpolarized cross-section and double-spin observables and is, most likely, responsible for the discrepancy between two methods of measurements of the proton form factors. We review different methods of calculations of the TPE amplitudes in the framework of the "hadron" and "quark-gluon" approaches. We discuss the dispersion approach suitable for low and intermediate Q^2, which includes elastic and inelastic intermediate hadronic states, as well as the connection of TPE with the proton radius puzzle. The present situation with direct experimental searches for the TPE amplitude in the e^+p/e^-p charge asymmetry is also discussed, as well as attempts to extract the TPE amplitudes from existing experimental data obtained by the Rosenbluth and double polarization techniques. The TPE physics in other processes such as elastic μp, e-nucleus, and $e\pi$ scattering is also reviewed.

K e y w o r d s: two-photon exchange, elastic scattering, proton form factors.

1. Introduction

Understanding the internal structure of a proton, neutron, and other strongly interacting systems was, for a long time, one of the fundamental problems of particle physics. Experiments on the elastic and inelastic scattering of ultra-relativistic electrons on nucleons and nuclei provide a unique tool for such a study.

Early experiments with the scattering of relativistic electron beams on hadron systems were done under the leadership of Robert Hofstadter in the 1950s at High Energy Physics Laboratory (HEPL) at Stanford [1] and gave information on the radii of a wide spectrum of nuclei, as well as the electric charge distribution in them.

Later on, the same method was used to measure the proton size. The proton radius of 0.77 fm, extracted in 1955 from the cross-sections of elastic electron-proton scattering with the electron beams of energies up to 550 MeV [2], testified irrefutably that the proton is not an "elementary" particle and has internal structure. A lot of interesting information on this stage of experiments at HEPL is contained in the review paper by Hofstadter [3].

After that, a lot of experiments were done to measure the proton size more accurately. The present measurements give 0.8775(51) fm for the proton radius from the electron-proton scattering [4] and 0.84087(39) fm from atomic transitions in the muonic hydrogen [5, 6]. The cause for the difference between these data is not yet clear and is discussed intensively in the literature (very recently, the results were published [7], where the value of

0.831(7)(12) fm was obtained from ep scattering at very low Q^2).

The first information on the internal magnetic structure of the neutron was reported in 1958 [8]. Subsequent studies of the electron scattering, which were carried out in various world facilities in next decades, provide a further detailed information about the internal structure of various strongly interacting systems such as nucleons, pions, and nuclei.

Because of the smallness of the fine structure constant α, theoretical interpretation of experimental data was mainly done in the lowest order in α or one-photon exchange (OPE) approximation (meaning the exchange of only one virtual photon between the scattered electron and the target). A fundamental ingredient of such model is the hadron electromagnetic (e.m.) current. In turn, the hadron current involves e.m. form factors (FFs), the main objects containing the information about the e.m. structure of a hadron system.

Due to the 1/2 spin of a nucleon, its e.m. current is described by two FFs F_1 and F_2, called Dirac and Pauli FFs or by linear combinations of F_1 and F_2, the electric and magnetic FFs, G_E and G_M. To separate the FFs, two different techniques are used, the Rosenbluth separation method [9], which is based on the cross-section data, and the double polarization technique elaborated at the Thomas Jefferson National Accelerator Facility (JLab for short) [10–13].

Up to the late 1990s, only the unpolarized ep cross-sections were measured. The Rosenbluth separation of those data had suggested that the nucleon FFs fulfil the approximate scaling

$$G_{Ep} \approx G_{Mp}/\mu_p \approx G_{Mn}/\mu_n, \tag{1}$$

where μ_p and μ_n are the proton and neutron magnetic moments. Double polarization experiments carried out at JLab since 1998 have changed the situation drastically, the ratio $\mu_p G_{Ep}/G_{Mp}$ measured by this method was shown to decrease linearly with Q^2. Because radiative corrections for the Rosenbluth and polarization techniques are different, the discrepancy of $\mu_p G_{Ep}/G_{Mp}$ can be naturally explained as the effect of radiative corrections. The theoretical analysis has shown that the two-photon exchange (TPE), whose contribution was ignored in the previous calculations, may be responsible for the discrepancy [14, 15].

The review is organized as follows. Sections 2, 3, and 4 have introductory purpose: we discuss the methods of proton FF measurements, OPE and TPE approximations, and the general structure of the TPE amplitude for the elastic ep scattering. Section 5 deals with calculations of the imaginary part of the TPE amplitude and applications to single spin asymmetries. Section 6 reviews different approaches to the calculation of the real part of the TPE amplitude at both hadronic and QCD levels. Sections 7 and 8 are devoted to the discussion of the status of experimental searches for the direct TPE effects and extraction of the TPE amplitude from experimental data on the ep scattering. TPE in other processes (μp scattering, electron scattering off the lightest nuclei, and the $e\pi$ scattering) is shortly reviewed in Sec. 9. The Appendix contains a collection of formulae for TPE contributions to various observables.

2. Born Approximation and Proton Form Factors

The main process of our interest will be the elastic electron-proton scattering:

$$\mathrm{e}^- + \mathrm{p} \to \mathrm{e}^- + \mathrm{p}. \tag{2}$$

Though we will consider other processes such as electron-neutron, electron-deuteron, and muon-proton scattering in some sections, we will mean, by default, the electron-proton case, unless explicitly noted otherwise.

For the convenience, we write down the definitions of all kinematic quantities, which are related to this process and will be used throughout the paper.

4-momenta of the initial and final particles will be denoted by k, k' for the electron and p, p' for the proton (the final ones are marked with the prime). The momentum transfer is

$$q = p' - p = k - k', \tag{3}$$

and its square $q^2 = t = -Q^2 < 0$. The electron and proton masses will be denoted by m and M, respectively. It is convenient to introduce vectors

$$K = \frac{1}{2}(k + k'), \quad P = \frac{1}{2}(p + p'), \tag{4}$$

for which

$$Kq = Pq = 0, \quad K^2 = m^2 - t/4, \quad P^2 = M^2 - t/4. \tag{5}$$

We also denote [1]

$$s = (k+p)^2, \quad u = (k'-p)^2, \quad \nu = s-u = 4PK. \quad (6)$$

In the first order of perturbation theory (Born or OPE approximation), the electron-proton scattering is described by the only Feynman diagram (Fig. 1). In this and all following diagrams, a thin line depicts an electron, thick line – proton, and wavy line – photon. Since the proton is not a point particle, the vertex corresponding to its interaction with the virtual photon (depicted as a gray circle in Fig. 1) should be written in the most general form

$$\Gamma_\mu(q) = F_1(q^2)\gamma_\mu - \frac{1}{4M}F_2(q^2)[\gamma_\mu, \hat{q}], \quad (7)$$

where $F_1(q^2)$ and $F_2(q^2)$ are some functions, which characterize the electromagnetic interaction of the proton – its form factors (FFs). F_1 and is called Dirac FF, and F_2 is called Pauli FF. Instead of F_1 and F_2, one often uses the linear combinations

$$G_E = F_1 + \frac{q^2}{4M^2}F_2 \quad \text{and} \quad G_M = F_1 + F_2, \quad (8)$$

– electric and magnetic FF, respectively [16]. The advantage of such choice of FFs will become evident below.

The amplitude corresponding to the diagram in Fig. 1 has the form

$$\mathcal{M}_1 = -\frac{4\pi\alpha}{q^2}\,\bar{u}'\gamma_\mu u\,\bar{U}'\Gamma^\mu(q)U, \quad (9)$$

where u', U' and u, U and bispinors of the final and initial particles, and Γ_μ is determined by Eq. (7). The cross-section of the unpolarized scattering calculated from amplitude (9) equals

$$d\sigma = \frac{2\pi\alpha^2 dt}{E^2 t}\frac{1}{1-\varepsilon}\left(\varepsilon G_E^2 + \tau G_M^2\right), \quad (10)$$

where $\tau = -t/4M^2$, E is the energy of the initial electron in the laboratory frame, and

$$\varepsilon = \left[1 + 2(1+\tau)\,\mathrm{tg}^2\,\tfrac{\theta}{2}\right]^{-1} = \frac{\nu^2 - Q^2(4M^2+Q^2)}{\nu^2 + Q^2(4M^2+Q^2)}, \quad (11)$$

[1] NB: in papers of other authors ν sometimes denotes the four times smaller quantity, $\nu = PK$.

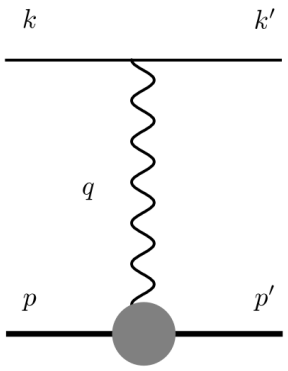

Fig. 1. First-order diagram

where θ is the scattering angle in that frame. The quantities E, θ, and τ are related by

$$E(E-2M\tau) = \frac{M^2\tau}{\sin^2\theta/2}. \quad (12)$$

The quantity ε, which varies from 0 to 1, characterizes the relative contribution of the longitudinal and transverse photons to the cross-section: the contribution of the transverse photons is independent of ε, and that of the longitudinal ones is proportional to it.

Equation (10), which was first derived (in a somewhat different form) in work [9], is called the Rosenbluth formula. From this equation, we see rationale behind the FF choice in the form (8): it contains only squares of the FFs and no interference terms.

Since FFs depend on t, but not on ε, the expression

$$\sigma_R = \varepsilon G_E^2 + \tau G_M^2, \quad (13)$$

which is called a reduced cross-section, is a linear function of ε regardless of the actual FFs.

This is the basis of the Rosenbluth method for the extraction of FFs from the experimentally measured cross-sections. The method requires the measurements to be performed at fixed t and several different values of ε. The resulting values of σ_R are plotted against ε, and should form the straight line. Then the line slope gives us the electric FF, and the intercept gives the magnetic FF. The linearity of the plot was, until recently, considered as a sign of the Born approximation validity.

The Rosenbluth method is very simple and was widely used for the determination of FFs of nucleons and light nuclei (such as ^{3}He) from the 1960s till today. But unfortunately, it has the following drawback: the error in the electric FF rapidly increases

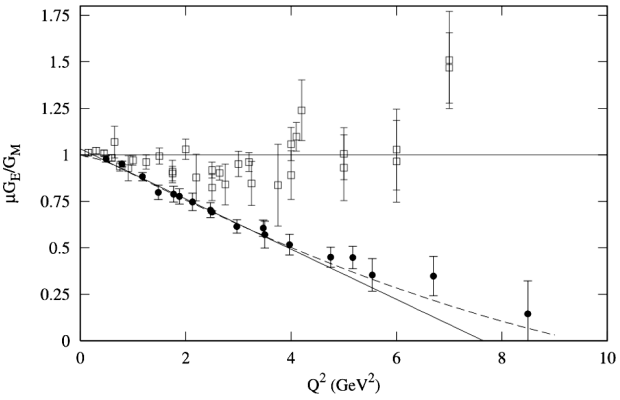

Fig. 2. Experimentally measured proton FF ratio. Squares – Rosenbluth method [21–24], circles – polarization transfer method [11, 13, 25, 26]. Blue line – Eq. (17), dashed line – parametrization from [27]

with the momentum transfer. Indeed, since the coefficient in front of G_M^2 in Eq. (13) becomes large, whereas $0 \le \varepsilon \le 1$, the main contribution in σ_R comes from the second term. Thus, the relative error $\Delta G_E/G_E$, which, in the order of magnitude, equals $\Delta\sigma_R/\sigma_R\,\sigma_R/G_E^2 = \Delta\sigma/\sigma\,\sigma_R/G_E^2$, will be much larger than the relative error of the cross-section $\Delta\sigma/\sigma$.

Thus, at large momentum transfers, it is more convenient to use another method, the polarization transfer method. It was proposed in the 1970s [17,18] and first used in an experiment in 1998 [19].

This method is based on the fact that if the beam electrons are longitudinally polarized, the recoil protons become polarized as well. Their spin orientation depends on the FF ratio G_E/G_M, which allows one to measure this ratio directly. Namely, if the initial electrons have the helicity λ, then the polarization 4-vector of the final protons is

$$S = S_\parallel \xi_\parallel + S_\perp \xi_\perp = \\ = \frac{-\lambda\sqrt{1-\varepsilon^2}}{\varepsilon G_E^2 + \tau G_M^2}\left(\tau G_M^2 \xi_\parallel + \sqrt{\frac{2\varepsilon\tau}{1+\varepsilon}} G_M G_E \xi_\perp\right), \quad (14)$$

where $\xi_\parallel$ and $\xi_\perp$ are unit vectors

$$\xi_\parallel = \frac{2M}{\sqrt{-q^2P^2}}\left(\frac{P^2}{M^2}\,p' - P\right), \\ \xi_\perp = \frac{\nu P - 4P^2 K}{\sqrt{P^2(\nu^2 + 4q^2P^2)}}, \quad (15)$$

such that $\xi_\parallel^2 = \xi_\perp^2 = -1$, $\xi_\parallel p' = \xi_\perp p' = \xi_\parallel \xi_\perp = 0$. Thus, the FF ratio is expressed via the ratio of longitudinal and transverse polarization components:

$$\frac{G_E}{G_M} = \sqrt{\frac{\tau(1+\varepsilon)}{2\varepsilon}}\,\frac{S_\perp}{S_\parallel}. \quad (16)$$

Note that, contrary to the Rosenbluth method, the polarization transfer method does not allow one to determine G_E and G_M separately. It is also more complicated technically, since it requires a polarized electron beam and a measurement of the proton polarization. On the other hand, since only the *ratio* of the polarization components is measured, there is no need to know the beam polarization, or analyzing power of the detector exactly. The main advantage of the method is that the ratio G_E/G_M is determined with higher accuracy, especially at large momentum transfers.

From the theoretical point of view, the method equivalent to the polarization transfer one is the beam-target asymmetry method [20], though the experimental setup is quite different. Longitudinally polarized electrons are scattered on the polarized protons, and one observes the asymmetry $A = \frac{\sigma_+ - \sigma_-}{\sigma_+ + \sigma_-}$, where $\sigma_\pm$ is the cross-section for the scattering of electrons with the helicity $\pm 1/2$.

In the Born approximation, A is also expressed via the FF ratio. Using the time reversal symmetry, one can show that the results obtained with this method should be identical to the results of the polarization transfer method, even beyond the Born approximation. Further, for brevity, we will speak of the polarization transfer method, implying the beam-target asymmetry method as its special case.

Proton FFs, obtained by the Rosenbluth method, approximately obey the relation $\mu G_E/G_M \approx 1$, where μ is the proton magnetic moment. The polarization transfer measurements were first performed at small Q^2 and confirmed this relation [19]. But when the momentum transfer values were increased up to $Q^2 \gtrsim 1$ GeV^2, the results become unexpected: the ratio G_E/G_M decreased monotonically as Q^2 increased and obviously disagreed with values obtained by the Rosenbluth method. Since then, several other experiments were performed by both methods, in which the accuracy was improved, and higher momentum transfers were reached (Q^2 up to 8.5 GeV^2, Fig. 2). The values of G_E/G_M, obtained by different authors by the same method, agree with one another well, whereas the values obtained by different

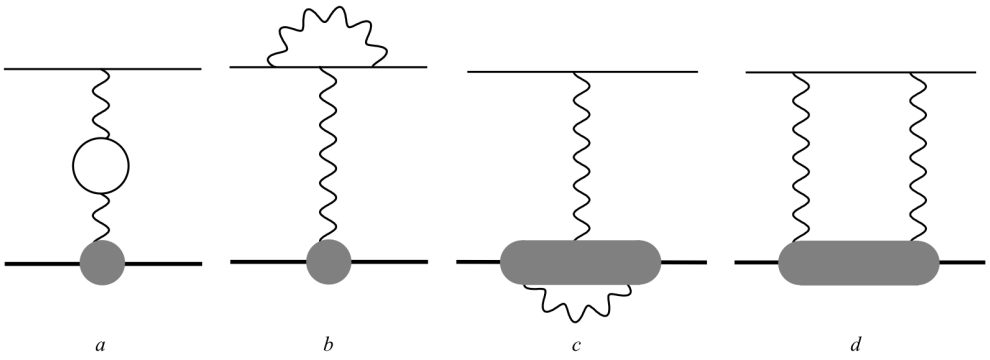

Fig. 3. Second-order diagrams

methods, significantly disagree. In particular, the ratio G_E/G_M, measured by the polarization transfer method at not very high Q^2, was well described by a linear function [28]

$$\mu G_E/G_M = 1 - 0.135(Q^2 - 0.24) \tag{17}$$

(solid line in Fig. 2).

One should note that such asymptotic behavior of the FFs contradicts the results obtained in the framework of QCD. Perturbative QCD calculations yield the dependence $F_1 \sim Q^2 F_2$ at large Q^2, which is equivalent to $G_E/G_M \sim$ const [29, 30].

The more accurate statistical analysis confirmed the above-mentioned statements. In particular, it was shown in Ref. [28] that

• the cross-sections measured in the Rosenbluth method do not contain rough errors;

• the cross-section measured in different experiments are consistent with each other;

• there is no statistically sound parametrization of FFs compatible with the results obtained by both methods.

This led to the suggestion that if we exclude a possibility of the rough error in the polarization transfer measurements, the discrepancy is likely caused by the terms of the next (second) order of perturbation theory which were neglected, when deriving Eqs. (13) and (16).

3. Second-Order Perturbation Theory

In the second order of perturbation theory, several Feynman diagrams exist (Fig. 3): vacuum polarization (3, *a*), electron-photon and proton-photon vertex corrections (3, *b* and 3, *c*, respectively), and TPE diagram (3, *d*). We do not draw a diagram analogous to 3d with crossed photon lines, since we treat its lower part as already symmetrized with respect to the photon interchange.

These diagrams have some new properties, which were absent in the Born approximation.

First, there is the so-called infra-red (IR) divergence. The integrals corresponding to diagrams in Fig. 3, *b, c, d* are logarithmically divergent, when the virtual photon momenta go to zero. Thus, with regard for these diagrams, the elastic scattering cross-section becomes infinite. It is well known that this stems from the incorrect formulation of the problem. Since any detector has a finite energy resolution, it is impossible for the experiment to separate the elastic process from the process with the additional emission of any number of soft photons with a total energy less than some threshold.

Thus, the true observable is only $\sigma(\Delta E)$ – the cross-section of such process, in which the sum of final electron and proton energies differs from the initial energy by not more than some $\Delta E > 0$.

This cross-section is convenient to calculate in the following way. Suppose that the photon has small but non-zero mass λ. Then all IR-divergent integrals become finite, but instead contain terms proportional to $\ln \lambda$. The cross-section $\sigma(\Delta E)$ is a sum of two quantities: the elastic scattering cross-section σ_{el} and the soft photon emission cross-section $\sigma_\gamma(\Delta E)$. Either of these quantities is divergent as $\lambda \to 0$, but the divergent terms exactly cancel in the sum, and the quantity $\sigma(\Delta E)$ appears well-defined as $\lambda \to 0$.

The form of the IR-divergent terms can be determined without calculation of the scattering amplitude and even without the expansion in α [31]. Indeed, if the quantity ΔE is small, then the photon emission

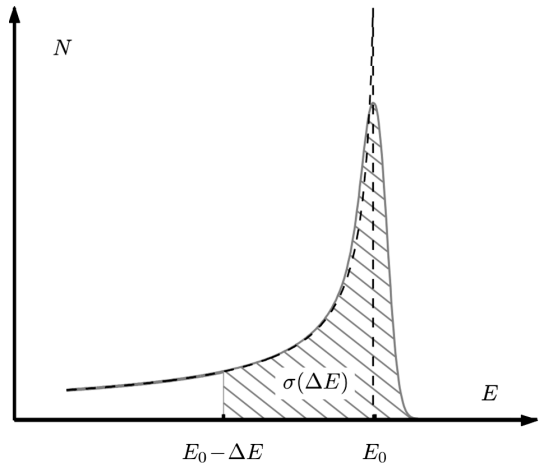

Fig. 4. Number of the events N depending on the final energy of particles E in the elastic scattering experiment

follows classical electrodynamics, and the photons are emitted independently of one another. The number of these photons will be a Poisson-distributed random quantity; the probability of the scattering with emitting exactly n photons equals

$$w_n = \frac{1}{n!} w^n \exp(-w),$$

where w is the probability of a photon emission:

$$w = \frac{\alpha}{\pi}\left(B_1 \ln\frac{\Delta E}{\lambda} + B_2\right), \tag{18}$$

where B_1 and B_2 are some functions of the particle momenta, which are known explicitly. So, we have a relation between the cross-section of the scattering with the emission of an arbitrary number of photons $\sigma(\Delta E)$ and the cross-section of the "elastic" scattering, i.e., without any emission $\sigma_{\rm el}$:

$$\sigma_{el} = w_0 \sigma(\Delta E) = \exp(-w)\sigma(\Delta E) \tag{19}$$

or

$$\sigma(\Delta E) = \sigma_{\rm el} \exp\left[\frac{\alpha}{\pi}\left(B_1 \ln\frac{\Delta E}{\lambda} + B_2\right)\right]. \tag{20}$$

We see that, for the IR-divergences to cancel, the quantity $\sigma_{\rm el}$ must have the form

$$\sigma_{\rm el} = \sigma_0 \exp\left[\frac{\alpha}{\pi}\left(B_1 \ln\frac{\lambda}{E} + B_3\right)\right], \tag{21}$$

where σ_0 is independent of λ. Then

$$\sigma(\Delta E) = \sigma_0 \exp\left[\frac{\alpha}{\pi}\left(B_1 \ln\frac{\Delta E}{E} + B_2 + B_3\right)\right]. \tag{22}$$

The auxiliary quantity λ disappears from the formulae, but instead the cross-section becomes dependent on ΔE. The cross-section of exactly elastic scattering, i.e., $\lim\limits_{\Delta E\to 0}\sigma(\Delta E)$, is zero. This is clear from the physical grounds: every collision of charged particles is accompanied by the emission of the electromagnetic waves, that is, soft photons.

Expanding (21) in series in α, one can find the IR-divergent terms in $\sigma_{\rm el}$ in every order of perturbation theory. They cancel with similar terms in the soft photon emission cross-section $\sigma_\gamma(\Delta E) = \sigma(\Delta E) - \sigma_{\rm el}$.

Then, what quantity is really measured in the experiments on the elastic scattering? Aside from minor details, which can differ between experiments, the elastic cross-section measurement is performed in the following way. For every scattering event, the energy E of the final particles (the electron and the proton) is determined. The typical histogram of E is shown in Fig. 4, E_0 is the initial energy. (E can be greater than E_0 because of the beam non-monochromaticity, finite detector resolution, and so on. The ideal experiment would yield the dashed curve; the solid curve, obtained in the real experiment is a convolution with a sort of "instrument function"). Then one chooses some ΔE, and all events with $E > E_0 - \Delta E$ are formally counted as elastic. The corresponding cross-section $\sigma(\Delta E)$ is proportional to the hatched area in Fig. 4 and is called the "uncorrected" or "measured" cross-section. Then the experimenters, starting from the measured quantity $\sigma(\Delta E)$, try to calculate the elastic scattering cross-section *in the Born approximation*, which is finally published as "the elastic cross-section with radiative corrections" ("corrected cross-section") $\sigma_{\rm cor}$. The quantity $\sigma(\Delta E) - \sigma_{\rm cor}$ is called the radiative correction and includes both the cross-section of the soft photon emission and the higher-order corrections to the elastic cross-section $\sigma_{\rm el}$. It can reach 20–30% (see, e.g., [21]).

It is clear that the radiative corrections are to be calculated theoretically. The standard procedure for this calculation was published in Ref. [32] and is based on the results of Ref. [33]. Most of the experimental works, especially older ones, used this procedure. Let us consider it in more details.

For the vacuum polarization and electron-photon vertex correction (3, *a* and 3, *b*), one uses the exact expressions obtained in QED [31]:

$$\mathcal{M}_{2\rm a} = f_{\rm a}(q^2)\mathcal{M}_1, \quad \mathcal{M}_{2\rm b} = f_{\rm b}(q^2)\mathcal{M}_1, \tag{23}$$

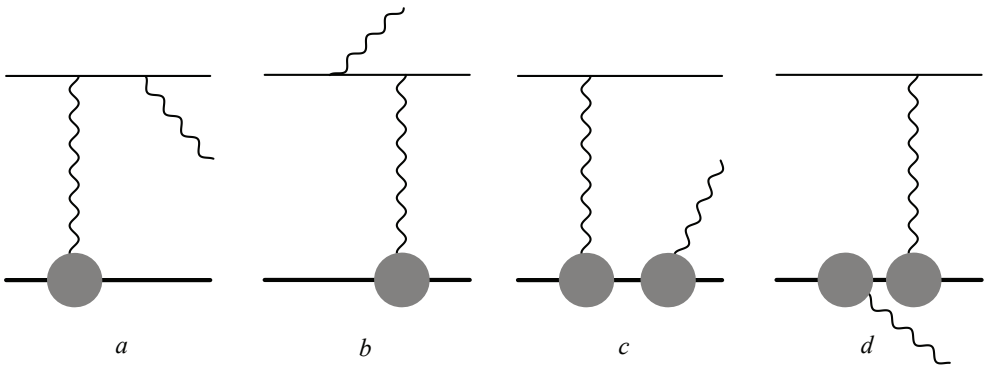

Fig. 5. Photon emission (bremsstrahlung) diagrams

where

$$f_{\rm a}(q^2) = \frac{\alpha}{3\pi} \ln \frac{-q^2}{m^2} \tag{24}$$

for diagram 3a and

$$f_{\rm b}(q^2) = -\frac{\alpha}{2\pi} \left(\frac{1}{2} \ln^2 \frac{-q^2}{m^2} + 2 \ln \frac{m}{\lambda} \ln \frac{-q^2}{m^2} \right) \tag{25}$$

for diagram 3, *b* (supposing that $-q^2 \gg m^2$). Due to the presence of the large logarithm $\ln \frac{-q^2}{m^2}$ in expressions (24, 25), these corrections may be quite large; in some high-energy experiments [21], the muon and hadron vacuum polarizations and higher order corrections to the electron-photon vertex were also taken into account.

Diagrams 3, *c* and 3 *d* in Refs. [32, 33] were calculated in the so-called soft photon approximation (or the Mo–Tsai approximation), that is, supposing that the momentum of one of the virtual photons is close to zero. In this way, one can exactly determine IR-divergent contribution, which must cancel the same term in the inelastic cross-section.

However, even if we forget the above, diagrams 3, *a*–*c* cannot cause the discrepancy between the Rosenbluth and polarization transfer methods in the measurements of the FFs. The point is that they all has the structure analogous to the Born amplitude, namely

$$\mathcal{M} = -\frac{4\pi\alpha}{q^2} \bar{u}' \gamma_\mu u \, \bar{U}' \delta\Gamma^\mu(q) U, \tag{26}$$

where

$$\delta\Gamma_\mu(q) = \delta F_1(q^2)\gamma_\mu - \frac{1}{4M} \delta F_2(q^2)[\gamma_\mu, \hat{q}]. \tag{27}$$

Thus, the inclusion of these diagrams does not break the formulae obtained in the Born approximation, but leads only to the effective change $F_i \to F_i + \delta F_i$. Thus, though the results obtained by both methods may change, the change will be the same, and the discrepancy cannot arise.

So, we end up with the conclusion that the only non-trivial diagram, which can be responsible for the discrepancy, is the TPE diagram (Fig. 3, *d*). The effect of TPE reveals itself in three ways:

- first, the amplitude has a non-zero imaginary part, which gives rise to such effects as single-spin asymmetries (absent in OPE);
- second, there is a correction to the real part of the amplitude, which now has a different tensor structure than in OPE, consequently breaking the Rosenbluth formula;
- third, the TPE correction has opposite signs for the $e^- p$ and $e^+ p$ scattering, which leads to the *charge asymmetry*: the cross-sections for the electron and positron scattering are now different.

Note that, in the Mo–Tsai soft-photon approximation, the diagram in Fig. 3, *d* has the same factorization property as other three: it is proportional to the OPE amplitude:

$$\mathcal{M}_{\rm 2d}^{\rm (Mo\text{-}Tsai)} = f_{\rm d}(\nu, q^2) \mathcal{M}_1. \tag{28}$$

Thus, the non-trivial TPE effects come not just from the TPE diagram, but from its IR-finite hard-photon part $\mathcal{M}_{\rm 2d} - \mathcal{M}_{\rm 2d}^{\rm (Mo–Tsai)}$.

Another component that could contribute to the discrepancy between the Rosenbluth and polarization transfer methods is higher order (in ΔE) corrections to the bremsstrahlung cross-section $\sigma_\gamma(\Delta E)$, which, in the leading order in α, is described by the diagrams in Fig. 5. This was addressed in Refs. [34, 35], where

the radiation by the electron (Fig. 5, *a, b*) was thoroughly studied in a model-independent way; and in Ref. [36], where the radiation by the proton was studied in the next-to-leading order in ΔE, and it was shown that, at least at high Q^2, these corrections are smaller than TPE and do not influence the experimental results noticeably. Thus, we will concentrate further on TPE corrections only.

4. Structure of the TPE Amplitude

In the general case, the elastic scattering of two nonidentical particles with spin 1/2 such as an electron and a proton is described by six scalar functions – invariant amplitudes, which may be taken as, for example, helicity amplitudes [31]. However, the typical energies involved in the electron-proton scattering experiments are several orders of magnitude greater than the electron mass, thus the latter can be safely neglected. Then the electron helicity is conserved, and the number of amplitudes decreases to three, which can be chosen as in [15]:

$$\mathcal{M} = -\frac{4\pi\alpha}{q^2}\bar{u}'\gamma_\mu u \times$$
$$\times \bar{U}'\left(\gamma^\mu \tilde{F}_1 - \frac{1}{4M}[\gamma^\mu, \hat{q}]\tilde{F}_2 + \frac{P^\mu}{M^2}\hat{K}\tilde{F}_3\right)U. \qquad (29)$$

The invariant amplitudes or generalized FFs, $\tilde{F}_i$ are functions of two kinematic variables, $\nu = 4PK$ and $t = q^2$. In the Born (OPE) approximation, the dependence on ν disappears, and the amplitudes reduce to the usual FFs:

$$\tilde{F}_1^{(\mathrm{Born})}(\nu, t) = F_1(t),$$
$$\tilde{F}_2^{(\mathrm{Born})}(\nu, t) = F_2(t),$$
$$\tilde{F}_3^{(\mathrm{Born})}(\nu, t) = 0$$

(compare (29) with (7) and (9)). The TPE diagram gives a contribution of order $O(\alpha)$ to each of these amplitudes. It is clear that one can choose any three independent linear combinations of $\tilde{F}_i$ as invariant amplitudes. Some authors introduce, in analogy with the electric and magnetic FFs, the quantities

$$\tilde{G}_M = \tilde{F}_1 + \tilde{F}_2 \quad \text{and} \quad \tilde{G}_E = \tilde{F}_1 - \tau\tilde{F}_2.$$

However, the most convenient choice of the amplitudes is, in our opinion, the following:

$$\mathcal{G}_E = \tilde{F}_1 - \tau\tilde{F}_2 + \nu\tilde{F}_3/4M^2, \quad \mathcal{G}_E^{(\mathrm{Born})} = G_E,$$
$$\mathcal{G}_M = \tilde{F}_1 + \tilde{F}_2 + \varepsilon\nu\tilde{F}_3/4M^2, \quad \mathcal{G}_M^{(\mathrm{Born})} = G_M, \qquad (30)$$
$$\mathcal{G}_3 = \nu\tilde{F}_3/4M^2, \quad \mathcal{G}_3^{(\mathrm{Born})} = 0.$$

Then, if the scattering amplitude has the general form (29), the unpolarized cross-section becomes

$$d\sigma = \frac{2\pi\alpha^2 dt}{E^2 t}\frac{1}{1-\varepsilon}\left(\varepsilon|\mathcal{G}_E|^2 + \tau|\mathcal{G}_M|^2 + \tau\varepsilon^2\frac{1-\varepsilon}{1+\varepsilon}|\mathcal{G}_3|^2\right). \qquad (31)$$

This formula is exact and does not rely on the expansion in α. We see that, in analogy with the Rosenbluth formula, there is no interference terms. Equation (14) for the final proton polarization in the polarization transfer method turns to be

$$S = \frac{-\lambda\sqrt{1-\varepsilon^2}}{\varepsilon|\mathcal{G}_E|^2 + \tau|\mathcal{G}_M|^2}\,\mathrm{Re}\,\tilde{G}_M^* \times$$
$$\times\left[\left(\mathcal{G}_M + \frac{\varepsilon(1-\varepsilon)}{1+\varepsilon}\mathcal{G}_3\right)\tau\xi_\parallel + \sqrt{\frac{2\varepsilon\tau}{1+\varepsilon}}\mathcal{G}_E\xi_\perp\right]. \qquad (32)$$

Contrary to the Born approximation, the amplitudes $\mathcal{G}$ in the general case are complex-valued. Their imaginary part is proportional to α and comes exclusively from the TPE diagram. On the other hand, Eqs. (31, 32), neglecting the terms of order $O(\alpha^2)$, contain only their real parts. This follows from the fact that the Born amplitudes are real; e.g.,

$$|\mathcal{G}_E|^2 = (G_E + \mathrm{Re}\,\delta\mathcal{G}_E)^2 + (\mathrm{Im}\,\delta\mathcal{G}_E)^2 =$$
$$= G_E^2 + 2G_E\,\mathrm{Re}\,\delta\mathcal{G}_E + O(\alpha^2),$$

where $\delta\mathcal{G}_E$ is the TPE amplitude. The imaginary part of the amplitudes gives rise to the new type of observables – single-spin asymmetries.

In the first order of perturbation theory, the final particles for the unpolarized scattering are unpolarized as well. If only one of the initial particles is polarized, the scattering cross-section is independent of its spin and still follows Eq. (10). The situation, where the spin of a polarized particle is perpendicular to the reaction plane, is of special interest. Since it has only two possible directions (say, up and down), we denote the corresponding cross-sections as $\sigma_\uparrow$ and $\sigma_\downarrow$ and define the asymmetry as

$$A_n, B_n = \frac{\sigma_\uparrow - \sigma_\downarrow}{\sigma_\uparrow + \sigma_\downarrow}. \qquad (33)$$

When the polarized particle is a proton (the target) this quantity is called a "target normal spin asymmetry" (TNSA) and denoted by A_n. For an electron,

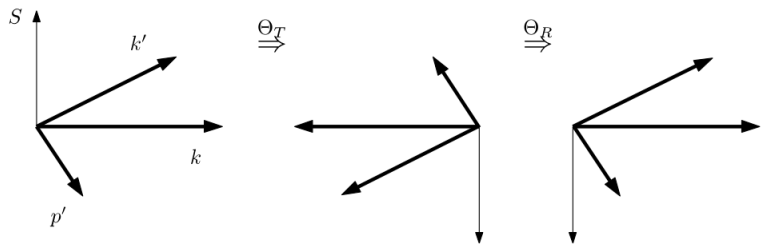

Fig. 6. To the derivation of the formula for TNSA

it is denoted by B_n and called a "beam normal spin asymmetry" (BNSA).

The interesting properties of these quantities are:

• as was stated above, both asymmetries are strictly zero in the OPE approximation; thus, the leading contribution to the asymmetry is given by TPE;

• they are expressed via the imaginary part of the scattering amplitude, which significantly simplifies theoretical calculations;

• the asymmetry does not contain IR divergencies. This can be inferred immediately from definition (33): both cross-sections, $\sigma_\uparrow$ and $\sigma_\downarrow$, contain the same IR-divergent factor (the exponent from Eq. (21)), which thus cancels. Therefore, there is no need for radiative corrections in the measurements of the asymmetry.

TNSA can be expressed via the amplitudes $\mathcal{G}$ introduced above as

$$A_n = \frac{\sqrt{2\tau\varepsilon(1+\varepsilon)}}{\tau G_M^2 + \varepsilon G_E^2} \times$$

$$\times \left[G_E \operatorname{Im}\left(\mathcal{G}_M + \frac{\varepsilon(1-\varepsilon)}{1+\varepsilon}\mathcal{G}_3 \right) - G_M \operatorname{Im}\mathcal{G}_E \right] + O(\alpha^2). \tag{34}$$

BNSA cannot be expressed via these amplitudes, since it vanishes for the zero electron mass. Thus, it also depends on the other three amplitudes, which were neglected in Eq. (29).

Single-spin asymmetries are considered in detail in Sec. 5.

Calculation of the whole TPE amplitude (and not just its imaginary part) is a difficult task. Early works considering TPE for the electron-proton scattering [37, 38] have the following common drawbacks:

• usually, the proton is considered as the source of a constant external field (static approximation, $M \to \infty$);

• only the cross-section correction is calculated, but not the scattering amplitude, which has three independent components (29).

The main difficulties with the rigorous calculation of the TPE amplitudes are the need to consider a large number of intermediate states and the FFs in the $\gamma^* p$ vertices.

5. Imaginary Part Effects

Let us demonstrate that the single-spin asymmetry (say, TNSA) defined according to Eq. (33) is proportional to the imaginary part of the TPE amplitude [39].

Denote the initial state by $|i\rangle$ and the final state by $|f\rangle$; the same states with the spins reversed are marked by a hat: $|\hat{i}\rangle$ and $|\hat{f}\rangle$. Then the cross-sections of our interest are, up to a constant factor,

$$\sigma_\uparrow = \sum |T_{fi}|^2, \quad \sigma_\downarrow = \sum |T_{f\hat{i}}|^2 = \sum |T_{\hat{f}\hat{i}}|^2, \tag{35}$$

where $\sum$ means the summation over the spins of the initial and final electrons and the final proton. Acting on the states $|i\rangle$ and $|f\rangle$ by the time reversal operator (Θ_T) and rotating around the normal to the scattering plane by 180° (Θ_R), see Fig. 6, we have

$$\Theta_R\Theta_T|i\rangle = \eta_i|\hat{i}\rangle, \quad \Theta_R\Theta_T|f\rangle = \eta_f|\hat{f}\rangle, \tag{36}$$

where $\eta_{i,f}$ are some phases, $|\eta_{i,f}|^2 = 1$. From the T-invariance of the electromagnetic interaction, it follows that

$$T_{\hat{f}\hat{i}} = \eta_i\eta_f^* T_{if}. \tag{37}$$

With the help of Eq. (37), the cross-section difference can be written as

$$\sigma_\uparrow - \sigma_\downarrow = \sum \left[|T_{fi}|^2 - |T_{if}|^2 \right] =$$

$$= \frac{1}{2}\sum \Big[(T_{fi}^* + T_{if})(T_{fi} - T_{if}^*) -$$

$$-(T^*_{if}+T_{fi})(T_{if}-T^*_{fi})\Big] =$$
$$= \frac{1}{2}\sum\Big[(T^*_{fi}+T_{if})(T_{fi}-T^*_{if}) -$$
$$-(T^*_{f\hat{i}}+T_{\hat{i}f})(T_{f\hat{i}}-T^*_{\hat{i}f})\Big].$$

The unitarity condition says

$$T_{fi}-T^*_{if} = i\sum_n T_{fn}T^*_{in}, \tag{38}$$

where the summation goes over the complete set of intermediate states n. In the case of electromagnetic interaction, the T-matrix elements are proportional to the small quantity α. This means that the T-matrix is Hermitian in the first order in α:

$$T^{(1)}_{fi} = T^{(1)*}_{if}, \tag{39}$$

and the anti-Hermitian part (which is usually somewhat inaccurately called "imaginary") arises only in the second order:

$$T_{fi}-T^*_{if} = i\sum_n T^{(1)}_{fn}T^{(1)}_{in} + O(\alpha^3). \tag{40}$$

Inserting (40) in (38), we see that, in the first non-vanishing order in α, the asymmetry has the form

$$A_n \approx i\sum_n \frac{\sum T^{(1)}_{fn}\left(T^{(1)}_{ni}T^{(1)}_{if} - T^{(1)}_{n\hat{i}}T^{(1)}_{\hat{i}f}\right)}{\sum\left(|T^{(1)}_{fi}|^2+|T^{(1)}_{f\hat{i}}|^2\right)}. \tag{41}$$

Of course, a similar equation holds for BNSA (when the polarized particle is an electron).

The outer summation in Eq. (41) goes over all states n that can be produced in the interaction of the electron with the proton. In the first order in α, they must consist of the electron and some hadronic state with baryon number 1, charge +1, and invariant mass $W \le \sqrt{s}$. This hadronic state can be bare proton, proton plus some number of mesons (πp, $\pi\pi p$, ηp...) or proton-antiproton pairs ($pp\tilde{p}$), *etc.* The contribution of the bare proton as the intermediate hadronic state is called the elastic contribution (as the production of this state would be the elastic process); other contributions are called inelastic.

The main problem in calculations of the asymmetry comes from the inelastic contribution, since, at not-so-small energies, the number of allowed intermediate states can be large. Therefore, one has to use some model for these states.

5.1. TNSA

TNSA was first considered in Refs. [39, 40]. The elastic part was calculated directly, and the inelastic part was constrained using a sort of the Cauchy inequality:

$$\left|T_{fi}-T^*_{if}\right| = \left|\sum_n T_{fn}T^*_{\rm in}\right| \le$$
$$\le \sqrt{\sum_n |T_{fn}|^2 \sum_n |T_{\rm in}|^2} \sim \sqrt{\sigma_f\sigma_i}, \tag{42}$$

where σ_i (σ_f) is the total inelastic cross-section from the state i (f).

The advantage of such approach is that the above expression includes only experimentally measurable quantities. Thus, the constraint is model-independent. However, as was already noted by the authors, while the bound given by Eq. (42) for the near-forward scattering is likely a good approximation to the imaginary part of the amplitude, for the large-angle scattering, it probably far overestimates its true value. Thus, we need to do a more accurate estimate of the inelastic contribution to TNSA.

Such calculations were performed in Refs. [41, 42]. In Ref. [41], the intermediate states included in the unitarity relation were πN states. These are the lowest inelastic states possible (other inelastic states include $\pi\pi N$, $\pi\pi\pi N$, ηN, and so on, and their contribution was neglected). The amplitudes of the pion electroproduction $\gamma^* N \to \pi N$, which enter the unitarity condition in this case, are reasonably well-known and were taken from the MAID model [43].

In Ref. [42], the lowest resonances were used instead, namely, $P_{33}(1232)$, $D_{13}(1520)$, $S_{11}(1535)$, $F_{15}(1680)$, and $P_{11}(1440)$, with transition amplitudes fitted from the experimental data. Compared to Ref. [41], on the one hand, we include some states other than πN, since the resonances are not 100% composed of πN. But, on the other hand, we leave out the nonresonant pion production.

It was found that the contributions of the resonances tend to cancel one another, and, for the larger energies, the asymmetry (and the imaginary part of the TPE amplitude as well) is dominated by the elastic part. Since the real and imaginary parts of the amplitude are connected via dispersion relations, it was suggested that the elastic contribution is a good approximation for the real part of the TPE amplitude as well.

5.2. BNSA

The BNSA is proportional to the lepton mass and vanishes in the $m \to 0$ limit. Indeed, a state with the electron spin perpendicular to the scattering plane is the superposition of the states with positive and negative helicities with the coefficients differing only in phase. But the helicity of a massless particle is conserved. Thus, there is no interference between different helicities, and the cross-sections $\sigma_\uparrow$ and $\sigma_\downarrow$ are equal.

However, numerically, the asymmetry is not as small as one may expect, since it contains logarithmic ($\ln Q^2/m^2$) and double-logarithmic ($\ln^2 Q^2/m^2$) enhancements, as was shown in Refs. [44–46]. The interplay between these terms is such that $\ln Q^2/m^2$ term dominates at forward angles and the $\ln^2 Q^2/m^2$ term at backward ones, because of different powers of Q^2 in front of the logarithms.

The following representation of BNSA can be easily derived from Eq. (41):

$$B_n = \frac{i\alpha q^2 m}{2\pi^2 D}\int \frac{d^3k''}{2\epsilon''}\frac{1}{q_1^2 q_2^2} Y(W, q_1^2, q_2^2) + o(m), \quad (43)$$

where the function $Y(W, q_1^2, q_2^2)$ is a contraction of the leptonic and hadronic tensors describing the virtual Compton scattering, but their exact forms are not needed here, $W = (p + k - k'')^2$ is the invariant mass of the hadronic intermediate state, and $D = \frac{4(2s+q^2-2M^2)^2}{4M^2-q^2}(4M^2G_E^2 - q^2G_M^2) + 4q^2(4M^2G_E^2 + q^2G_M^2)$. The double-logarithmic terms found in Ref. [46] arise from the approximate formula

$$\int \frac{d^3k''}{2\epsilon''}\frac{1}{q_1^2 q_2^2} Y(W, q_1^2, q_2^2) \approx \frac{\pi}{4Q^2} Y(\sqrt{s}, 0, 0) \ln^2 \frac{Q^2}{m^2}, \quad (44)$$

which yields

$$B_n \approx B_n^{(\ln^2)} = -\frac{i\alpha m}{8\pi D} Y(\sqrt{s}, 0, 0) \ln^2 \frac{Q^2}{m^2}. \quad (45)$$

The following properties of these double-logarithmic contributions are notable: it is produced by the intermediate states with the maximal kinematicly possible invariant mass, $W = \sqrt{s}$. Therefore, the elastic contribution does not take part here, and the energy dependence of the asymmetry has resonance form with maxima at the positions of prominent resonances.

The double-logarithmic contribution has the following asymptotics at small Q^2:

$$B_n^{(\ln^2)} \sim Q^3 \ln^2 \frac{Q^2}{m^2}. \quad (46)$$

in agreement with the results of Ref. [45].

Another approach was used in Ref. [44]. While, in Ref. [46], we searched for the terms with the highest power of the large logarithm, the authors of Ref. [44] searched for the slowest-decreasing terms at $Q \to 0$. The result was the following:

$$B_n \approx B_n^{(\ln)} = -\frac{2m(s-M^2)^2}{\pi^2 D} \times \times \left(G_E + \frac{Q^2}{4M^2}G_M\right) Q \ln \frac{Q^2}{m^2}\, \sigma_{\rm tot}, \quad (47)$$

where $\sigma_{\rm tot}$ is the total photoabsorption cross-section on the proton, i.e., the cross-section of the reaction $\gamma p \to X$.

Note that Eqs. (47) and (45) are distinct contributions and should, in general, be added together. The approximation of Eq. (47) is valid for very small scattering angles,

$$\sin^2 \frac{\theta}{2} \ln \frac{Q^2}{m^2} \ll 1, \quad (48)$$

while the double-logarithmic approximation of Eq. (45) is valid upon the reverse condition

$$\sin^2 \frac{\theta}{2} \ln \frac{Q^2}{m^2} \gg 1. \quad (49)$$

6. Calculation of the TPE Amplitude

The calculation of the real part of the TPE amplitude is a more complicated task, since the intermediate hadronic state is here virtual and, regardless of the total energy, states of all masses can contribute. There are two main ways of such calculation: "hadronic" approach (Sec. 6.1) and "parton-quark" one suitable for high Q^2 (Sec. 6.2).

6.1. Hadronic approach

The "hadronic" approach implies that the intermediate states in the lower part of the diagram in Fig. 3, *d* are sets of hadrons. Certainly, the unlimited number of variants is possible here, and just the lowest-mass states are usually taken into account.

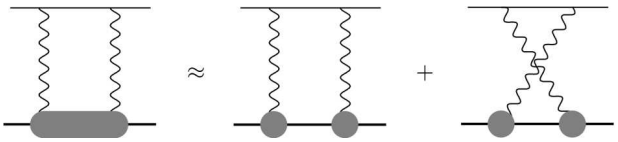

Fig. 7. The elastic contribution

As with the calculation of the imaginary part, we distinguish the "elastic contribution", which arises, when the intermediate state is the proton itself, and the inelastic one coming from all other intermediate states. The elastic contribution is easier to calculate, and, in many situations, it is the dominant one. In addition, the IR-divergent terms in the amplitude come exclusively from the elastic contribution; the inelastic one is always IR-finite. Only the elastic contribution is to be considered for the $e\mu$ (instead of ep) scattering, which was done in Ref. [47].

The difference of the ep scattering from the $e\mu$ case is that the proton has an internal structure. Thus, the question arises: what are its propagator and the $pp\gamma$ vertex function? It was argued that since one of the protons entering the vertex, is virtual, it should differ from the usual $pp\gamma$ e.m. vertex and contain the so-called off-shell FFs, which are not known experimentally.

Nevertheless, as an approximation, the TPE diagram was calculated in Ref. [14, 48] under assumption that the proton propagator is the same as that of a point Dirac particle, and the $pp\gamma$ vertex coincides with the usual on-shell one:

$$\Gamma_\mu(q) = F_1(q^2)\gamma_\mu - \frac{1}{4M}F_2(q^2)[\gamma_\mu, \hat{q}]. \tag{50}$$

This expression was chosen, because it preserves the gauge invariance, while another common one, equivalent in the case of on-shell proton,

$$\Gamma_\mu(q) = (F_1 + F_2)\gamma_\mu - F_2\frac{(p+p')_\mu}{2M} \tag{51}$$

does not. This approximation is schematically depicted in Fig. 7: the full TPE contribution is approximated by the sum of two diagrams called the "box" and "crossed-box" diagrams. They are related by the crossing symmetry. Thus, the scattering amplitude is

$$\mathcal{M} = \mathcal{M}^{(\mathrm{box})} + \mathcal{M}^{(\mathrm{xbox})} = \mathcal{M}^{(\mathrm{box})}(\nu, t) - \mathcal{M}^{(\mathrm{box})}(-\nu, t). \tag{52}$$

Some technical details of the calculation are given below.

6.1.1. Elastic contribution

The expression corresponding to the box diagram in Fig. 7 is

$$i\mathcal{M}^{(\mathrm{box})} = \left(\frac{\alpha}{\pi}\right)^2 \int d^4k'' \times$$
$$\times \frac{\bar{u}'\gamma_\mu(\hat{k}'' + m)\gamma_\nu u\, \bar{U}'\Gamma_\mu(q_2)(\hat{p}'' + M)\Gamma_\nu(q_1)U}{q_1^2 q_2^2 (k''^2 - m^2)(p''^2 - M^2)}. \tag{53}$$

First, the γ-matrix structure of the formula must be reduced to that of Eq. (29). This can be done in two stages. It is well known that any product of γ matrices can be represented as a linear combination of the 16 structures: 1, γ_μ, $[\gamma_\mu, \gamma_\nu]$, $\gamma_5\gamma_\mu$, and γ_5. Then we use the fact that, in Eq. (53), those matrices are sandwiched between on-shell particle spinors. It can be shown that

$$\frac{1}{2}q^2\, \bar{u}'\gamma_5\gamma_\mu u = -mq_\mu\, \bar{u}'\gamma_5 u - i\epsilon_{\mu\nu\sigma\tau}K^\sigma q^\tau\, \bar{u}'\gamma^\nu u,$$
$$\frac{1}{4}q^2\, \bar{u}'[\gamma_\mu, \gamma_\nu]u = -i\epsilon_{\mu\nu\sigma\tau}K^\sigma q^\tau\, \bar{u}'\gamma_5 u + \tag{54}$$
$$+ m\,(q_\mu \bar{u}'\gamma_\nu u - q_\nu \bar{u}'\gamma_\mu u) + \bar{u}'u\,(K_\mu q_\nu - K_\nu q_\mu).$$

(and similarly for the proton spinors, with the replacement $K_\mu \to P_\mu$, $q_\mu \to -q_\mu$, $m \to M$). Using these identities, $\mathcal{M}$ can be represented as a linear combination of the four structures of the form

$$\bar{u}'\gamma_\mu u\, \bar{U}'\gamma_\nu U, \quad \bar{u}'\gamma_5 u\, \bar{U}'\gamma_\mu U,$$
$$\bar{u}'\gamma_\mu u\, \bar{U}'\gamma_5 U, \quad \text{and} \quad \bar{u}'\gamma_5 u\, \bar{U}'\gamma_5 U.$$

The 2nd and 3rd combinations would violate the T-invariance and thus do not actually appear; and the last combination does not appear due to the negligibly small electron mass.

Now, the task is to calculate the coefficients in front of these structures and to compare the resulting amplitude with Eq. (29) to obtain generalized FFs. The combinations that would violate the T invariance automatically receive zero coefficients after the integration.

At this stage, we obtain, for the generalized FFs, expressions like

$$\delta\mathcal{G} = \sum_{i,j=1}^{2} \int d^4k'' \frac{F_i(t_1)F_j(t_2)}{t_1 t_2} \times$$
$$\times \left[\frac{A_{ij}(t_1, t_2, \nu, t)}{(k''^2 - m^2)(p''^2 - M^2)} + \frac{A_{k,ij}(t_1, t_2, \nu, t)}{k''^2 - m^2} + \right.$$
$$\left. + \frac{A_{p,ij}(t_1, t_2, \nu, t)}{p''^2 - M^2} + A_{1,ij}(t_1, t_2, \nu, t)\right], \tag{55}$$

which contain elastic proton FFs F_i. The functions A_{ij} are polynomials in t_1 and t_2 and rational functions of ν. To proceed further, the FFs are parametrized as a sum of fixed poles:

$$\frac{F_i(t)}{t} = \sum_a \frac{c_{ia}}{t - m_a^2}. \tag{56}$$

Integral (55) is then represented as a linear combination

$$\delta\mathcal{G} = \sum_{ijab} c_{ia} c_{jb} \int \frac{d^4k''}{(t_1 - m_a^2)(t_2 - m_b^2)} \times$$
$$\times \left[\frac{A_{ij}(m_a^2, m_b^2, \nu, t)}{(k''^2 - m^2)(p''^2 - M^2)} + \frac{A_{k,ij}(m_a^2, m_b^2, \nu, t)}{k''^2 - m^2} + \right.$$
$$\left. + \frac{A_{p,ij}(m_a^2, m_b^2, \nu, t)}{p''^2 - M^2} + A_{1,ij}(m_a^2, m_b^2, \nu, t) \right]. \tag{57}$$

The integrals

$$\int \frac{d^4k''}{(t_1 - m_a^2)(t_2 - m_b^2)(k''^2 - m^2)(p''^2 - M^2)},$$
$$\int \frac{d^4k''}{(t_1 - m_a^2)(t_2 - m_b^2)(k''^2 - m^2)},$$
$$\int \frac{d^4k''}{(t_1 - m_a^2)(t_2 - m_b^2)},$$

entering Eq. (57) are known as 4-point, 3-point, and 2-point functions, respectively [49], and can be calculated either analytically or numerically.

Finally, the IR-divergent contribution should be subtracted (see also discussion in Sec. 3). It is equal to

$$\delta\mathcal{G}_E^{(\mathrm{IR})} = f^{(\mathrm{IR})} G_E, \quad \delta\mathcal{G}_M^{(\mathrm{IR})} = f^{(\mathrm{IR})} G_M, \quad \delta\mathcal{G}_3^{(\mathrm{IR})} = 0, \tag{58}$$

where the factor $f^{(\mathrm{IR})}$ depends on the particular method of calculation of radiative corrections. In the prescription of Mo–Tsai [32], which was widely used in experiments, it is equal to

$$f^{(\text{Mo-Tsai})} = \frac{\alpha}{\pi} \left[\ln \frac{4M^2\lambda^2}{\nu^2 - t^2} \ln \frac{\nu - t}{\nu + t} - \right.$$
$$\left. - \mathrm{Li}_2\left(1 - \frac{\nu - t}{2M^2}\right) + \mathrm{Li}_2\left(1 - \frac{\nu + t}{2M^2}\right) \right]. \tag{59}$$

In some recent experiments, the so-called Maximon–Tjon prescription [50] is used instead of the Mo–Tsai one, which (naturally) has the same divergent part, but differs from the latter in finite terms:

$$f^{(\mathrm{MT})} = \frac{\alpha}{\pi} \ln \frac{\lambda^2}{-t} \ln \frac{\nu - t}{\nu + t}. \tag{60}$$

6.1.2. Time-like region problem

However, there is a problem within this approach, which was pointed out in Ref. [51]. The procedure, described above involves the FF fitting. But the FFs are measured experimentally only in the space-like region ($Q^2 > 0$). Naturally, the fit is done over that region only. In the time-like region ($Q^2 < 0$), the difference between the actual FFs and the fit can be significant. But the integration in Eqs. (53, 55) goes over both space-like and time-like regions. Therefore, the results of calculations using such fit are doubtful.

To overcome this problem, another method of integration was used in Ref. [51]. Using the analytic properties of FFs, Eq. (55) was transformed via the Wick rotation, resulting in the other integral containing FFs for space-like Q^2 only:

$$\delta\mathcal{G} = \sum_{i,j=1}^{2} \int\limits_{t_1, t_2 \le 0} \mathcal{K}_{ij}(t_1, t_2) F_i(t_1) F_j(t_2) dt_1 dt_2, \tag{61}$$

where $\mathcal{K}_{ij}(t_1, t_2)$ are certain known functions.

This result implies that the fitting of FFs in the space-like region only is fine, as long as the analytic structure of FFs is preserved by the fit, i.e., all singularities lie on the negative real axis. In this case, the integral effectively depends on FFs at $Q^2 > 0$ only.

Trying the calculation with different FF parametrizations, it was found that the results are almost insensitive to it.

6.1.3. Dispersion approach

However, the problem of the off-shell FFs remained unsolved. To resolve this problem, the dispersion method was proposed [52].

The idea is that, at first, the imaginary part of the TPE amplitude is calculated. This is done with the help of the unitarity condition (40), where the intermediate states are on-shell. Therefore, one can employ usual FFs measured experimentally.

Then the real part of the amplitude is reconstructed via the dispersion relations, and it appears that (in the case of single-particle intermediate state, either elastic or inelastic one) such reconstruction can be done analytically and independently of particular FFs.

Calculations with this method were first done for the elastic intermediate state [52]. It was found

that the elastic contribution calculated in Ref. [52] within the dispersion approach differs from the results of Refs. [48, 51], but the difference is very small numerically.

6.1.4. Inelastic contribution

Later on, the calculations like [48] were performed for the inelastic contribution: namely, $\Delta(1232)$ [53] and higher resonances [54] as intermediate states. The width of resonances was neglected: they were considered as zero-width particles with proper spin-parity and on-shell transition FFs. For their propagators, the usual propagators of spin-1/2 and spin-3/2 particles were used.

The results indicated that the contributions of resonances are smaller than the elastic one, the largest of them is the $\Delta(1232)$ contribution, and the contributions of different resonances have different signs, partly cancelling each other.

The approach of Ref. [51] can also be applied in this case, showing that it is still sufficient to fit the transition amplitudes at $Q^2 > 0$ only [55].

However, it is clear that neglecting the resonance width completely is not a good idea, as the width may be even comparable to mass (as in Röper resonance $N^*(1440)$); also the problem of the proper choice of a propagator and transition FFs remains unsolved. Thus, the dispersion approach of Ref. [52] was applied to the calculation of the inelastic contribution. In Ref. [56], the contribution of the zero-width Δ resonance was calculated within this approach. Moreover, in Ref. [57], the full P_{33} channel of the πN system was included, effectively considering the Δ resonance with a realistic width and shape (as Δ almost 100% consists of πN). In Ref. [58], the same approach was used to include all πN states with spin 1/2 and 3/2 (namely, S_{11}, S_{31}, P_{11}, P_{31}, P_{13}, P_{33}, D_{13} and D_{33} channels). Here, the πN system with c.m. energy W was treated as a single particle with proper spin-parity, mass W, and transition FFs derived from the pion photoproduction amplitudes, which, in turn, were taken from the MAID model [43].

The results were the following. At small Q^2, the inelastic contribution to TPE amplitudes is very small (negligible compared to the elastic one); at intermediate energies it has the resonance shape with maxima near the positions of prominent resonances, which are sharp, if we neglect resonance width (Ref. [56]) and become smooth, if we properly account it (Refs. [57, 58]); and, at high Q^2, it is gradually growing with Q^2.

The main contribution among all inelastic channels comes from the P_{33} channel, where $\Delta(1232)$ lives, and overall larger contributions come from the channels with quantum number of lightest resonances.

Though the TPE corrections to the cross-section and to the magnetic FF are dominated by the elastic contribution, it was found that the agreement with experimental data is improved, by taking the inelastic contribution into account.

It was also found that the correction to the G_E FF due to inelastic states is relatively large, growing almost linearly with Q^2 at $Q^2 \gtrsim 2$ GeV^2, and soon exceeds the elastic one.

6.2. High Q^2

At high Q^2, the hadronic approach becomes doubtful, because a large number of intermediate states is involved. On the other hand, at high Q^2, the proton-virtual photon interaction can be treated with the help of special technics developed for that case: generalized parton distributions (GPDs) and perturbative quantum chromodynamics (pQCD).

The GPD is a generalization of parton distribution functions, which are used in describing the deep inelastic scattering [59]. In the GPD model of Refs. [60, 61], both virtual photons interact with the same quark (on the contrary, such diagrams in pQCD are suppressed by a factor α_s, since they need an extra gluon to be exchanged between quarks, see below). The TPE amplitude is obtained as a convolution of the TPE amplitude of the elastic electron-quark process with the distribution of quarks in proton – GPD. The authors of Refs. [60, 61] claim that the diagrams, in which two photons interact with different quarks, are "subleading in Q^2 because of the momentum mismatches in the wavefunctions".

The pQCD can be used, in particular, to describe high-Q^2, high-energy exclusive reactions with hadrons such as the elastic lepton scattering [29]. Though the straightforward application of pQCD yields results, which are not very consistent with the experiments (in particular, the magnetic FF of a proton becomes zero, and that of a neutron turns positive), it was shown that introducing the phenomenological quark distribution amplitude allows one to

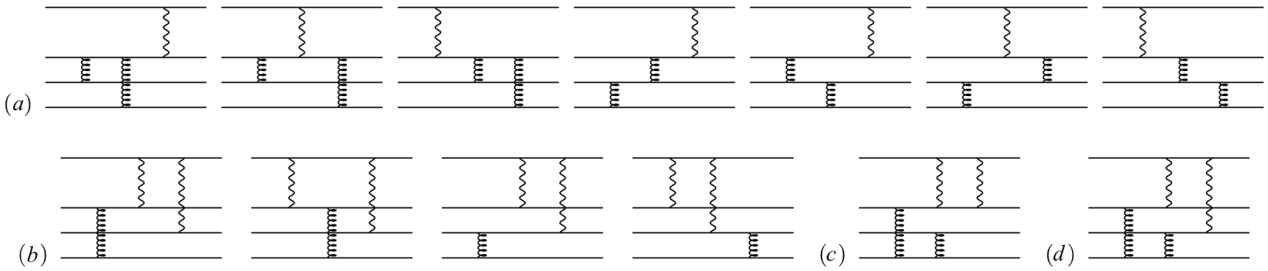

Fig. 8. pQCD diagrams for $eN \to eN$: OPE (a), TPE, leading order (b), subleading order (c, d)

obtain a reasonable agreement at currently accessible experimental energies. In the pQCD approach, the scattering amplitude is split into a hard "core", which describes the scattering off a set of (asymptotically free) quarks, and calculated according to the QCD perturbation theory, and quark distribution amplitudes, which connect physical hadron with multiquark states and are determined empirically with the help of various sum rules.

The pQCD representation of TPE has an important feature: comparing pQCD diagrams for OPE (Fig. 8, a) and TPE (Fig. 8, b), one can see that the former includes 1 photon and 2 gluon exchanges, producing a factor of $\alpha\alpha_s^2$, whereas, for the TPE, we have 2 photons and 1 gluon, which gives a factor of $\alpha^2\alpha_s$. In this way in pQCD, the ratio TPE/OPE is of order α/α_s, which is much larger than naive α, and raises with Q^2, as α_s decreases.

In Ref. [62], the TPE corrections to the elastic eN scattering were calculated in the leading-order pQCD. In this approximation, only the non-spin-flipping amplitudes exist – $\delta\mathcal{G}_M$ and $\delta\mathcal{G}_3$, whereas $\delta\mathcal{G}_E$ (as G_E itself) cannot be assessed: they are subleading-order effects. It is convenient to use normalized TPE amplitudes: $\delta\mathcal{G}_M/G_M$ and $\delta\mathcal{G}_3/G_M$, where both numerator and denominator are calculated according to pQCD. This way, we also avoid the uncertainty coming with the absolute normalization of the quark distribution amplitudes.

The results are:

$$\left(\frac{\delta G_M}{G_M}, \frac{\delta\mathcal{G}_3}{G_M}\right) = -\frac{3\alpha}{\alpha_s}\frac{\langle\phi(y_i)|(T_{\delta G_M}, T_{\delta\mathcal{G}_3})|\phi(x_i)\rangle}{\langle\phi(y_i)|T_{G_M}|\phi(x_i)\rangle}, \quad (62)$$

with

$$T_{G_M} = (1+h_1h_3)\left[\frac{2e_1}{x_3y_3(1-x_1)^2(1-y_1)^2} + \right.$$
$$+ \frac{2e_1}{x_2y_2(1-x_1)^2(1-y_1)^2} +$$
$$+ \frac{e_2}{x_1y_1x_3y_3(1-x_1)(1-y_3)} -$$
$$- \frac{e_1}{x_2y_2x_3y_3(1-x_1)(1-y_3)} -$$
$$\left. - \frac{e_1}{x_2y_2x_3y_3(1-x_3)(1-y_1)}\right], \quad (63)$$

$$T_{\delta G_M} = \frac{e_1e_2(1-h_1h_3)}{x_2y_2x_3y_3(1-x_2)(1-y_2)} \times$$
$$\times \frac{(\nu-q^2)/(1-x_2) + (\nu+q^2)/(1-y_2) - 2\nu}{\nu(x_2-y_2) - q^2(x_2+y_2-2x_2y_2) + i0}, \quad (64)$$

$$T_{\delta\mathcal{G}_3} = \frac{e_1e_2(1-h_1h_3)}{x_2y_2x_3y_3(1-x_2)(1-y_2)} \times$$
$$\times \frac{2\nu}{\nu(x_2-y_2) - q^2(x_2+y_2-2x_2y_2) + i0}, \quad (65)$$

where $\phi(x_i) \equiv \phi(x_1, x_2, x_3)$ are quark distribution amplitudes, e_i are quark charges, and h_i are doubled helicities. Soon afterwards, the same results were obtained in Ref. [63].

Main features of this result are:

• the TPE amplitude is proportional to α/α_s, which means approximately the logarithmic growing with Q^2;

• it has the identical ε-dependence at any fixed Q^2;

• absence of the IR divergence – it is easy to see that IR-divergent terms are subleading in α_s;

• the main contribution in pQCD regime comes from the area, where both virtual photons are hard, $Q_1^2 \sim \sim Q_2^2 \sim Q^2$.

It was also shown that the results of the "hadronic" and pQCD approaches are compatible with each other at lower Q^2, and a rather smooth transition from the "hadronic" to pQCD regime seems to occur at $Q^2 \gtrsim 3$ GeV^2, Fig. 9.

In Ref. [64], the authors argued that, though the pQCD approach gives a good approximation of the "hard contribution", i.e., the contribution, where both

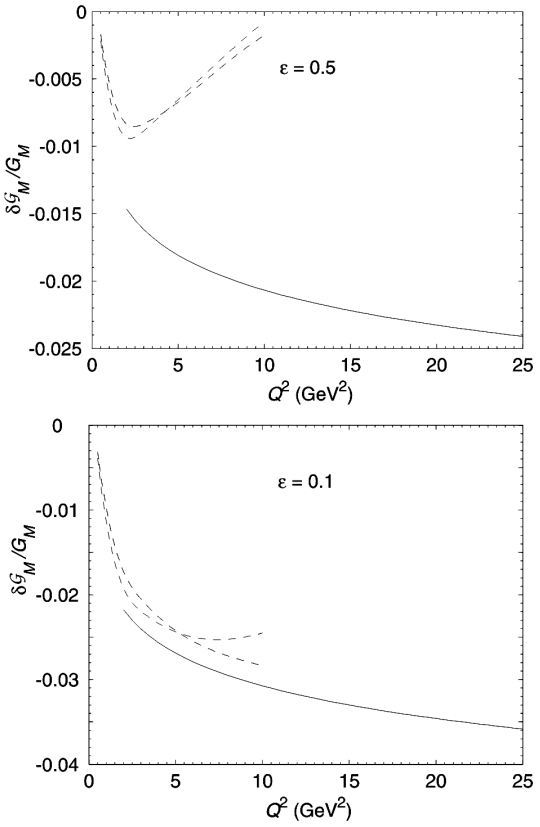

Fig. 9. TPE amplitude $\delta\mathcal{G}_M$ vs. Q^2 at $\varepsilon = 0.5$ (top) and $\varepsilon = 0.1$ (bottom). Dashed curves show "hadronic approach" calculations with two different FF parametrizations

virtual photons are hard, the "soft" contribution like one considered in Refs. [60, 61] is not negligible at the actual experimental kinematics and should be added. This idea was tried in Ref. [64], where the soft contribution was calculated in the so-called soft collinear exchange (SCET) approach.

6.3. Low Q^2 and proton radius

The behavior of TPE amplitudes at low Q^2 and energies is of special interest not only by itself, but also because this may affect the proton radius extraction.

The proton electric radius r_E is defined by

$$r_E^2 = -\frac{1}{6}\left.\frac{dG_E}{dQ^2}\right|_{Q^2=0} \tag{66}$$

and equals, in the nonrelativistic approximation, to the r.m.s. radius of the electric charge distribution inside a proton. This important quantity not only shows the proton "size", but influences other observables such as sizes of light nuclei, Lamb shift, and hyperfine splitting in hydrogen, *etc.* The similarly defined magnetic radius r_M gives r.m.s. radius of the magnetic moment distribution

$$r_M^2 = -\frac{1}{6}\left.\frac{dG_M}{dQ^2}\right|_{Q^2=0}. \tag{67}$$

The value of r_E is usually determined from the low-energy ep scattering, by measuring the G_E form factor at reasonably small Q^2 and extrapolating to $Q^2 = 0$ to find the derivative. This approach was, however, criticized in [65], since, on the one hand, at larger Q^2, the result is influenced by higher-order (in Q^2) terms, but, on the other hand, too low-Q^2 measurements are more prone to systematic errors.

If $Q^2 \to 0$ and $E \to 0$, the proton can be considered as a point particle, and the TPE reduces to the second Born approximation for the scattering in the Coulomb potential, which was studied long ago in Refs. [66, 67]. The corresponding contribution to the cross-section is sometimes called the "Coulomb correction":

$$\frac{\delta\sigma}{\sigma} = \alpha\pi\frac{\sin\frac{\theta}{2}}{1+\sin\frac{\theta}{2}}. \tag{68}$$

It was shown to affect the proton radius extraction [68]: after including the Coulomb corrections, r_E increased by $(0.008 - 0.013)$ fm depending on the fit strategy.

In a somewhat more precise approach, the proton is considered as a fixed source of the external electric field with the profile corresponding to its electric FF. Thus, the problem reduces to the relativistic electron scattering in the external potential. The second Born approximation for this process was studied in Ref. [69], where the cross-section in the general case and for some common potentials was obtained in the analytic form.

From numerical results discussed in Sec. 6 6.1, the TPE amplitude changes its sign at $Q^2 \sim 0.3$ GeV^2 and rather sharply grows at $Q^2 \to 0$. To prevent the misunderstanding, we note that, speaking of $Q^2 \to 0$, we mean $Q^2 \ll M^2$, but still $Q^2 \gg m^2$. Otherwise, our main approximation (ultrarelativistic electron) would not work. For $Q^2 \ll m^2$, the results would be quite different, and this is not discussed here.

In Ref. [70], the low-Q^2 limit for the real part of the TPE amplitudes was obtained from the general relativistic formulae via a limiting procedure. The results for $\mathcal{G}_E$ at $Q^2 \to 0$ are consistent with [66] (as, at small energies, the electric FF dominates the cross-section), whereas, for $\mathcal{G}_M$ and $\mathcal{G}_3$, they were new.

In Ref. [71], the TPE amplitudes were calculated via the nonrelativistic approach (of course, nonrelativistic refers to a proton and not to an electron), which, for the amplitude $\mathcal{G}_E$, is equivalent to the results of [69]; it was found that, at moderate Q^2, the real part of the amplitudes is described reasonably well. But, interestingly, the imaginary part strongly differs from the relativistic result, coinciding with it at $Q^2 \to 0$ only.

The full TPE correction (not just the Coulomb one) was applied during the extraction of a proton radius in [72] and [73]. Ref. [72] concludes that, numerically, the difference between full TPE and just Coulomb correction is small (+0.0015 fm to r_E). In Ref. [73], it was found that both electric and magnetic radii increase after taking TPE into account, r_E by ~ 0.01 fm and r_M by ~ 0.03 fm.

In the meantime, the proton electric radius was determined with the entirely different method: measuring the Lamb shift in muonic hydrogen [6]. Surprisingly, the obtained value of 0.841 fm was in the striking disagreement with the previous results from the *ep* scattering, 0.8768(69) fm [74]. This so-called "proton radius puzzle" gave rise to speculations, whether there is some peculiarity in the muon electromagnetic interaction, or the discrepancy is just a result of the poor consistency of the scattering approach. To explore the former possibility, a muon-proton scattering experiments were proposed [75], which, in turn, called for the estimate of TPE effects in the muon-proton scattering, discussed in Sec. 9.1.

On the other hand, the large experiment on the low-energy *ep* scattering was performed at Mainz Microtron [76]. Its results were, in general, consistent with previous electron scattering experiments and still in disagreement with new muon hydrogen data. In particular, the electric radius was found to be 0.879(8) fm. In addition, the authors found that, to achieve a consistency with the polarization experiments, some extra non-standard correction is required, which they cautiously interpret as "TPE or other physics" [77].

7. Experiments

A number of experiments were performed to see directly the TPE effects caused by the real part of the amplitude.

The GEp-2γ experiment [26] was aimed at observing the ε dependence of the proton FF ratio [2] $R = G_E/G_M$, measured via the polarization transfer method. Such dependence should constitute a clear sign of TPE. In terms of invariant amplitudes $\mathcal{G}$, the TPE correction to this ratio is

$$\frac{\delta R_{\rm exp}}{R_{\rm exp}} = \mathrm{Re}\left[\frac{\delta\mathcal{G}_E}{G_E} - \frac{\delta\mathcal{G}_M}{G_M} - \frac{\varepsilon(1-\varepsilon)}{1+\varepsilon}\frac{\delta\mathcal{G}_3}{G_M}\right]. \qquad (69)$$

The data were taken at fixed $Q^2 = 2.5$ GeV^2 and three different values of ε. In addition, the longitudinal polarization component, $S_\parallel$, of the final proton [3] was measured, where TPE correction is equal to [cf. Eq. (32)]:

$$\frac{\delta S_\parallel}{S_\parallel} = -2\varepsilon\,\mathrm{Re}\left[\frac{R^2}{\varepsilon R^2+\tau}\left(\frac{\delta\mathcal{G}_E}{G_E} - \frac{\delta\mathcal{G}_M}{G_M}\right) + \frac{\varepsilon}{1+\varepsilon}\frac{\delta\mathcal{G}_3}{G_M}\right]. \qquad (70)$$

Somewhat surprisingly, no ε dependence of R was seen in the experiment: the three measured values are almost the same (within 1.5% bounds). One possible cause for such outcome is that, near this kinematic point, the variation of the total (elastic + inelastic) TPE correction to G_E/G_M is minimal (Fig. 10). An experiment at higher Q^2 (e.g., Q^2= 3.5 GeV^2) with the same accuracy would clearly reveal the ε dependence caused by TPE.

For $S_\parallel$, some rise (about 2.3%) at higher ε was observed, but it should be noted that the point with the smallest ε was used for the normalization here, and, essentially, we remain with only two points, so it is hard to make any conclusions about the trend.

Several experiments were devoted to measuring the charge asymmetry, i.e., the e^+p/e^-p scattering cross-section ratio. Since the TPE correction has opposite signs for e^+p and e^-p, the deviation of the ratio from unity is a direct TPE effect and equals twice the cross-

[2] Throughout the paper, we denote $R = G_E/G_M$, but, in the literature. another definition is frequently used: $R = \mu G_E/G_M$ such that $R|_{Q^2\to 0} = 1$.

[3] Denoted by P_l in original papers.

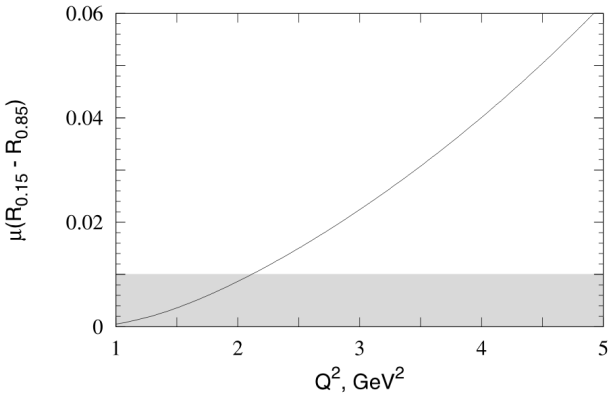

Fig. 10. Difference between the TPE correction to the measured $\mu R = \mu G_E/G_M$ at $\varepsilon = 0.15$ and $\varepsilon = 0.85$ versus Q^2 calculated according to [58]. Gray band at the bottom shows a typical error of the GEp-2γ experiment

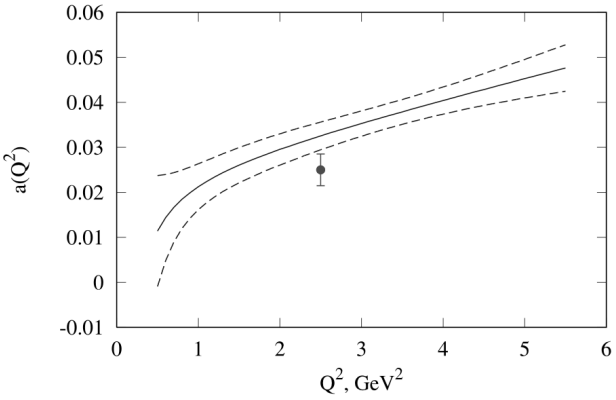

Fig. 11. Coefficient a, as determined in Refs. [82] (lines, $\pm 1\sigma$) and [83] (point)

section correction:

$$1 - R_{\pm} = 2\frac{\delta\sigma}{\sigma} = \frac{4}{\varepsilon R^2 + \tau}\,\mathrm{Re}\left[\varepsilon R^2 \frac{\delta\mathcal{G}_E}{G_E} + \tau\frac{\delta\mathcal{G}_M}{G_M}\right]. \tag{71}$$

In the VEPP-3 experiment [78], the ratio $R_{\pm}$ was measured at the beam energies $E = 1.0$ and 1.6 GeV, and several different angles, which correspond to Q^2 from 0.8 to 1.5 GeV^2 and ε from 0.27 to 0.45. The measured ratio $R_{\pm}$ was clearly larger than unity and agrees well with theoretical calculations [58].

In the CLAS experiment [79], two series of measurements were performed: at the fixed $Q^2 = 1.45$ GeV^2 and ε from 0.4 to 0.9 and at the fixed $\varepsilon = 0.88$ and Q^2 from 0.2 to 1.4 GeV^2. Though the results are rather close to 1 within errors, they show the 2.5σ preference to TPE over "no TPE" [79]; in Ref. [58], it was shown that the full TPE contribution (elastic + inelastic) is best consistent with data (has the least χ^2), the elastic only is slightly worse, and the worst is absence of TPE.

In the OLYMPUS experiment [80], the ratio was measured with $E = 2$ GeV electrons and positrons at Q^2 from 0.6 to 2.2 GeV^2 (ε from 0.4 to 0.9). It is of interest that the preliminary results in the region $\varepsilon \approx 0.8 - 0.9$ are below unity and, thus, contradict theoretical predictions from Refs. [48, 52, 58].

8. Extraction of TPE Amplitudes

When checking for TPE effects, another approach is possible: assuming that the scattering amplitude is a sum of OPE and TPE, and the discrepancy between the Rosenbluth and polarization methods is entirely due to TPE, one may try to extract the TPE amplitude directly from the experimental data. The thus extracted value will be model-independent and can be easily compared to the theoretical calculations.

The first attempts to do this were carried out in Refs. [15, 81]. However, the authors of that works arbitrarily assumed that only one of three TPE amplitudes, $Y_{2\gamma}$ ($\delta\mathcal{G}_3/G_M$ in our notation) is responsible for the discrepancy.

The rigorous application of such approach was done in [82]. Using the generalized FFs introduced in Eq. (30), one can see that at high and even at moderate Q^2, the TPE correction to the cross-section comes almost entirely from the magnetic FF:

$$\sigma_R = \varepsilon|\mathcal{G}_E|^2 + \tau|\mathcal{G}_M|^2 =$$

$$= \varepsilon G_E^2 + 2\varepsilon G_E\,\mathrm{Re}\,\delta\mathcal{G}_E + \tau\left[G_M^2 + 2G_M\,\mathrm{Re}\,\delta\mathcal{G}_M\right]. \tag{72}$$

The term with $\delta\mathcal{G}_E$ is the smallest one, since not only $\tau \equiv \frac{Q^2}{4M^2} \gg \varepsilon$, but also $G_E/G_M \approx 1/\mu_p \approx \approx 1/2.79$. Thus,

$$\sigma_R \approx \varepsilon G_E^2(Q^2) +$$

$$+ \frac{Q^2}{4M^2}\left[G_M^2(Q^2) + 2G_M(Q^2)\,\mathrm{Re}\,\delta\mathcal{G}_M(Q^2,\varepsilon)\right]. \tag{73}$$

Given the experimental fact that the Rosenbluth plots are linear (i.e., the reduced cross-section is a linear function of ε), one may conclude that $\delta\mathcal{G}_M$ should be an approximately linear function of ε. Additionally

recalling that the the dispersion relations require $\delta\mathcal{G}_M|_{\varepsilon=1} = 0$, we arrive at

$$\delta\mathcal{G}_M(Q^2,\varepsilon) = a(Q^2)(1-\varepsilon). \tag{74}$$

As a result, R_{LT}, the FF ratio measured within the Rosenbluth method becomes equal to

$$R_{LT}^2 = \frac{R^2 - 2a\tau}{\tau(1+2a)}, \tag{75}$$

where $R = G_E/G_M$ is the true FF ratio, and we can determine the coefficient a and the whole $\delta\mathcal{G}_M$ amplitude directly from the combination of Rosenbluth and polarization transfer data (the last point was missed in Refs. [82], but corrected in Ref. [83]).

After the GEp-2γ experiment [26], new precise data at $Q^2 = 2.5$ GeV^2 became available, and a new analysis was carried out in Refs. [83] and [84].

In Ref. [83], the slope of $\delta\mathcal{G}_M$ was determined from new data and again turned out to be in agreement with theoretical calculations. Another quantity measured in the experiment (longitudinal component of the final proton polarization, $S_\parallel$) gave an opportunity to determine $\delta\mathcal{G}_3$, though the precision was much worse here. In fact, the experimental value is compatible with zero. The third amplitude $\delta\mathcal{G}_E$ could not be determined accurately. But, basing on the fact that experimental R varies very little with ε, one can conclude that $\delta\mathcal{G}_E/G_E \approx \delta\mathcal{G}_M/G_M$.

A similar program was tried by the authors of Ref. [84]. To extract TPE amplitudes, they assumed a custom ε dependence of the final proton polarization $S_\parallel$. Nevertheless, their conclusion was that only one of three TPE amplitudes could be extracted reliably.

9. TPE in Other Processes

The previous sections were devoted mainly to the elastic electron-proton scattering (or, possibly, to the electron-nucleon scattering, since a neutron differs from a proton only in FFs). In this section, we will consider TPE in other processes. First, an electron can be replaced with a muon to see effects related to the lepton mass. Then we consider the electron scattering off various targets, in particular, on pions and light nuclei (deuteron, ^{3}He, ^{3}H). Other processes, for which TPE effects were studied, but will not be discussed here, include the electroproduction of pions [85] and Δ resonance [86], parity-violating ep scattering [87], and deep inelastic scattering [88].

9.1. Muon-proton scattering

After the discovery of the proton radius puzzle, one of the possible explanations was that the elecromagnetic (e.m.) interaction of a muon is in some way different from that of an electron. To test this possibility, it was proposed to measure the proton e.m. radius in the scattering approach, but with the muon beam [75].

In order to handle the results of such experiment, one should be able to calculate TPE corrections to the μp scattering. They were studied in Refs. [89, 90] and [91, 92]. The main difference between the ep and μp scattering is that the muon mass is not negligible. Therefore, there are six, not three, invariant amplitudes now:

$$\mathcal{M} = -\frac{4\pi\alpha}{q^2}\Big\{\bar u'\gamma_\mu u\,\bar U'\gamma_\nu U\Big[(F_1+F_2)g_{\mu\nu} - \\ - F_2\frac{P_\mu P_\nu}{M^2} + F_3\frac{P_\mu K_\nu}{M^2} + F_4\frac{K_\mu P_\nu}{m^2} - F_5\frac{K_\mu K_\nu}{m^2}\Big] - \\ - F_6\,\bar u'\gamma_5 u\,\bar U'\gamma_5 U\Big\}. \tag{76}$$

The properties of the parameter ε in the Rosenbluth formula are also changed: instead of (11), it now has the form

$$\varepsilon = \frac{\nu^2 - Q^2(4M^2+Q^2)}{\nu^2 + (Q^2-4m^2)(4M^2+Q^2)} \tag{77}$$

and, for fixed Q^2, varies not from 0 to 1, but between $2m^2/Q^2$ and 1; the near-forward scattering, as before, corresponds to $\varepsilon \to 1$.

The elastic contribution to TPE in the μp scattering for low momentum transfers was calculated in Ref. [90]. The same method as described in Sec.6 6.1 was used. It was found that the TPE correction to the cross-section is about 0.5% and several times smaller than for the ep scattering with similar kinematics, because the contribution of the lepton-spin-flipping amplitudes (F_4 and F_5; the amplitude F_6 does not contribute to the unpolarized cross-section) has different sign and partially cancels the spin-nonflipping amplitudes.

Later, the same authors developed a dispersion formalism to calculate TPE amplitudes for the μp scattering [93, 94]. It is worth to note that the calculation of the amplitude F_4 requires a subtracted dispersion relation.

9.1.1. Triangle diagram

In Refs. [91, 92], a completely new type of the TPE contribution (first mentioned in Ref. [95]) was considered: the triangle diagram, Fig. 12. It arises from the exchange of a single C-even meson, which then decays into two virtual photons. Certainly, it exists for the ep scattering as well, but is negligible there, because its contribution is proportional to the lepton mass. On the other hand, for the μp scattering, it cannot be left out, since the muon mass is larger by three orders of magnitude.

It it natural to expect that larger contributions would come from the lightest mesons, as the expression for the diagram contains the factor $1/(Q^2+\mu^2)$, originating from the meson propagator (where μ is the meson mass). The lightest candidate is π meson, but it was shown in Ref. [91] that the contribution of a pseudoscalar meson does not interfere with the OPE amplitude and thus has no effect in the unpolarized scattering. The next lightest meson is scalar $\sigma(500)$. Its contribution was estimated to be about 0.1% in the kinematics of the MUSE experiment [75]. It was also found that the contribution of the triangle diagram strongly grows as $Q^2 \to 0$.

In Ref. [92], the low-Q^2 behavior of the triangle diagram and its possible effect for the proton radius puzzle were studied. It was shown that the corresponding amplitude follows approximately the $a + b\sqrt{Q^2}$ formula, and the shift of the muon hydrogen energy levels induced by the diagram is about 30 times smaller than needed to resolve the discrepancy between different measurements of the proton radius.

9.2. TPE on nuclei

TPE in the elastic electron scattering off the light nuclei (d, ^{3}He, ^{3}H) was studied in Refs. [96–101].

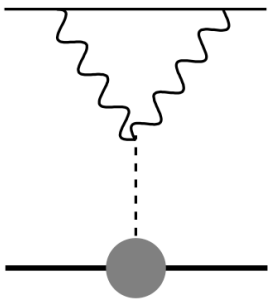

Fig. 12. Triangle diagram

The important point here is that the nuclear elastic FFs decline with Q^2 rather rapidly (exponentially). Therefore, the significance of TPE may be enhanced.

If we consider the elastic contribution only, then the nucleus is viewed as a single particle. However, the nuclear excited states are usually much closer to the ground state than for a proton, thus the inelastic contributions are probably important.

If we want go further and consider the inelastic contributions as well, we must account for the internal structure of a nucleus. At moderate energies, it is quite natural to view the nucleus as composed of nucleons and to neglect the quark degrees of freedom. Thus, similarly to the pQCD picture for a proton, there are two types of Feynman diagrams here: where both virtual photons interact with the same nucleon (type I) and where the photons interact with different nucleons (type II). In such calculations, the motion of the nucleons inside a nucleus is usually described in the nonrelativistic or semirelativistic approximation.

9.1.2. Spin-1/2 (^{3}He and ^{3}H)

The ^{3}He and ^{3}H nuclei consist of three nucleons and have spin 1/2, similarly to a proton. Thus, the general formula for the TPE amplitude (29) holds here as well: there are three independent TPE amplitudes.

The elastic contribution (i.e., ignoring the excitation of a nucleus) to the TPE for electron scattering off ^{3}He target was calculated in Refs. [48] and [71] using the same methods which were developed for the electron-proton scattering. In addition, the single spin asymmetries in the elastic $e-^3$He scattering were studied within same model in Ref. [100] and found to be rather large and momentum-transfer-dependent.

More thoroughly, the TPE amplitudes for the elastic electron-trinucleon scattering were studied in Ref. [101] using a semirelativistic nuclear wavefunction corresponding to the popular Paris and CD-Bonn nucleon-nucleon interaction potentials. It was found that the TPE corrections are several times larger than in the electron-proton scattering, and the diagrams of type II are dominant, except for the correction to the magnetic FF at large Q^2.

9.1.3. Deuteron

A deuteron has spin 1, and, thus, the structure of the scattering amplitude is different from the previous (spin-1/2) case. For the electron-deuteron scattering

in the OPE approximation, there are three FFs: electric G_C, quadrupole G_Q, and magnetic G_M; and in the general case, there are six FFs.

It was shown [98] that TPE can give large contributions (up to 10-20% at $Q^2 > 2.5$ GeV^2 [99]) to the elastic *ed* scattering cross-section, but it largely depends on the deuteron wave function at short distances, which is poorly known. It was also shown that the analyzed tensor component T_{22} is mainly determined by TPE at $Q^2 > 0.5$ GeV^2 [99].

TPE in the elastic *ed* scattering was also studied in the framework of the effective Lagrangian approach [96, 97]. The results were somewhat different. In particular, it was found that the largest effect of TPE is seen in the polarization observable T_{10} at small scattering angles.

9.3. TPE on a pion

TPE in the elastic electron-pion scattering is significantly simpler to study than in the electron-proton case. Since the pion is a spin-0 particle, for both OPE and TPE, there is only one invariant amplitude or FF, $F(q^2)$:

$$\mathcal{M} = -\frac{4\pi\alpha}{q^2}\bar{u}'\gamma_\mu u\,(p+p')_\mu\,F(q^2). \qquad (78)$$

Thus, the only effect of TPE is a correction to this FF (and its dependence on ε). The first calculations of this correction was done in Refs. [102, 103]. In both papers only the elastic contribution was considered; the authors of Ref. [103] additionally assumed that each of the virtual photons carries about a half of the transferred momentum, while the authors of Ref. [102] performed the full calculation of box and crossed-box diagrams via n-point functions (the approach similar to Ref. [48]). Numerically, the correction was found to be about 1%, smaller at small Q^2 and to increase at $Q^2 \gtrsim 1$ GeV^2, especially sharply at extreme backward angles.

It was argued in Ref. [104] that the virtual Compton scattering tensor implicitly used in these works breaks the gauge invariance, and the so-called contact term should be added to it. Numerically, however, the change turned out to be small.

In Ref. [105], the TPE correction to the pion FF was calculated using the appropriately modified dispersion approach of Ref. [52] with elastic and inelastic (ρ and b_1 mesons) intermediate states. The results for the elastic contribution were in agreement with previous works. The inelastic contribution was found to be negligible with respect to the elastic one for small Q^2 similarly to the *ep* case and becoming comparable to it at $Q^2 \gtrsim 2$ GeV^2, though being still smaller. It was also shown that the sharp growth of the high-Q^2 TPE amplitude at backward angles is due to the u-channel threshold singularity, which is close at $Q^2 \gg M^2$ to the boundary of the physical region.

10. Conclusions and Outlook

Since the discrepancy in proton FF measurements was revealed in the mid-2000s, our understanding of TPE and its role in the elastic *ep* scattering has advanced significantly. The methods were proposed to calculate TPE amplitudes at low and intermediate Q^2, including elastic and simplest inelastic intermediate hadronic states. The discrepancy is most likely explained by TPE; TPE amplitudes extracted from the combination of Rosenbluth and polarization transfer data agree with theoretical calculations.

At low Q^2, the TPE corrections influence the proton radius measurements both for the *ep* scattering and the Lamb shift in muonic hydrogen and should be taken into account in such experiments. For the high-Q^2 kinematics, QCD-based methods of TPE calculations are available.

Several targeted experiments on the e^+/e^- charge asymmetry in the elastic scattering show a clear preference to the "TPE" hypothesis over the "no TPE" one, but the further, more precise, measurements would be in order.

The failure to observe the expected TPE effect in GEp-2γ experiment is likely explained by the unfortunate choice of a kinematics. We suggest conducting a similar experiment at higher Q^2 (for instance, 3.5 GeV^2), which should be sufficient to see clearly the ε dependence of the polarization ratio.

In recent years, the theoretical understanding of TPE in the elastic muon-proton and electron-nucleus scattering was actively developed, and some work should still be done in these fields.

APPENDIX: TPE corrections to observables

In this section, the formulae for the TPE contributions to various observables of the elastic electron-proton scattering are gathered. The electron mass is neglected. The amplitudes $\delta\mathcal{G}_E$,

$\delta\mathcal{G}_M$, and $\delta\mathcal{G}_3$ are defined according to Eqs. (30, 29). In the following equations, $R = G_E/G_M$ and $\tau = Q^2/4M^2$.

The unpolarized cross-section and electron-positron cross-section ratio:

$$\frac{\delta\sigma}{\sigma} = \frac{1-R_{\pm}}{2} = \frac{2}{\varepsilon R^2+\tau}\,\mathrm{Re}\left[\varepsilon R^2\frac{\delta\mathcal{G}_E}{G_E}+\tau\frac{\delta\mathcal{G}_M}{G_M}\right]. \quad (79)$$

The FF ratio R_{exp}, as measured in the polarization transfer method:

$$\frac{\delta R_{\mathrm{exp}}}{R_{\mathrm{exp}}} = \mathrm{Re}\left[\frac{\delta\mathcal{G}_E}{G_E}-\frac{\delta\mathcal{G}_M}{G_M}-\frac{\varepsilon(1-\varepsilon)}{1+\varepsilon}\frac{\delta\mathcal{G}_3}{G_M}\right]. \quad (80)$$

The longitudinal component of the final proton polarization:

$$\frac{\delta S_{\parallel}}{S_{\parallel}} = -2\varepsilon\,\mathrm{Re}\left[\frac{R^2}{\varepsilon R^2+\tau}\left(\frac{\delta\mathcal{G}_E}{G_E}-\frac{\delta\mathcal{G}_M}{G_M}\right)+\frac{\varepsilon}{1+\varepsilon}\frac{\delta\mathcal{G}_3}{G_M}\right]. \quad (81)$$

Target normal spin asymmetry:

$$A_n = -\sqrt{2\varepsilon(1+\varepsilon)}\frac{R\sqrt{\tau}}{\varepsilon R^2+\tau}\times$$
$$\times\,\mathrm{Im}\left[\frac{\delta\mathcal{G}_E}{G_E}-\frac{\delta\mathcal{G}_M}{G_M}-\frac{\varepsilon(1-\varepsilon)}{1+\varepsilon}\frac{\delta\mathcal{G}_3}{G_M}\right]. \quad (82)$$

1. R. Hofstadter, R.W. McAllister. Electron scattering from the proton. *Phys. Rev.* **98**, 217 (1955).
2. E. Chambers, R. Hofstadter. Structure of the proton. *Phys. Rev.* **103**, 1454 (1956).
3. R. Hofstadter. Electron scattering and nuclear structure. *Rev. Mod. Phys.* **28**, 214 (1956).
4. R.J. Mohr, D.B. Newell, B.N. Taylor. CODATA recommended values of the fundamental physical constants: 2014. *Rev. Mod. Phys.* **88**, 035009 (2016).
5. R. Pohl *et al.* The size of the proton. *Nature* **466**, 213 (2010).
6. A. Antognini *et al.* Proton structure from the measurement of 2S-2P transition frequencies of muonic hydrogen. *Science* **339**, 417 (2013).
7. W. Xiong *et al.* A small proton charge radius from an electron-proton scattering experiment. *Nature* **575**, 147 (2019).
8. M.R. Yearian, R. Hofstadter. Magnetic form factor of the neutron. *Phys. Rev.* **110**, 552 (1958).
9. M.N. Rosenbluth. High Energy elastic scattering of electrons on protons. *Phys. Rev.* **79**, 615 (1950).
10. M.K. Jones *et al.* G_{E_p}/G_{M_p} ratio by polarization transfer in $\mathbf{e}p \to e\mathbf{p}$. *Phys. Rev. Lett.* **84**, 1398 (2000).
11. V. Punjabi *et al.* Proton elastic form-factor ratios to $Q^2 = 3.5$ GeV^2 by polarization transfer. *Phys. Rev. C* **71**, 055202 (2005).
12. O. Gayou *et al.* Measurement of G_{E_p}/G_{M_p} in $\mathbf{e}p \to e\mathbf{p}$ to $Q^2 = 5.6$ GeV^2. *Phys. Rev. Lett.* **88**, 092301 (2002).
13. A. Puckett *et al.* Final analysis of proton form factor ratio data at $Q^2 = 4.0$, 4.8 and 5.6 GeV^2. *Phys. Rev. C* **85**, 045203 (2012).
14. P.G. Blunden, W. Melnitchouk, J.A. Tjon. Two-photon exchange and elastic electron-proton scattering. *Phys. Rev. Lett.* **91**, 142304 (2003).
15. P.A.M. Guichon, M. Vanderhaeghen. How to reconcile the Rosenbluth and the polarization transfer methods in the measurement of the proton form factors. *Phys. Rev. Lett.* **91**, 142303 (2003).
16. R.G. Sachs. High-energy behavior of nucleon electromagnetic form factors. *Phys. Rev.* **126**, 2256 (1962).
17. A.I. Akhiezer, M.P. Rekalo. Polarization phenomena in the scattering of electrons by protons in the region of high energies. *Dokl. AN SSSR* **180**, No. 5, 1081 (1968).
18. A.I. Akhiezer, M.P. Rekalo. Polarization phenomena in the scattering of leptons on hadrons. *ÉChAYa* **4**, No. 3, 662 (1973).
19. B.D. Milbrath *et al.* Comparison of polarization observables in electron scattering from the proton and deuteron. *Phys. Rev. Lett.* **80**, 452 (1998).
20. M.K. Jones *et al.* Proton G_E/G_M from beam-target asymmetry. *Phys. Rev. C* **74**, 035201 (2006).
21. R.C. Walker *et al.* Measurements of the proton elastic form factors for $1 \le Q^2 \le 3$ (GeV/c)^2 at SLAC. *Phys. Rev. D* **49**, 5671 (1994).
22. L. Andivahis *et al.* Measurements of the electric and magnetic form factors of the proton from $Q^2 = 1.75$ to 8.83 (GeV/c)^2. *Phys. Rev. D* **50**, 5491 (1994).
23. M.E. Christy *et al.* Measurements of electron-proton elastic cross-sections for $0.4 < Q^2 < 5.5$ (GeV/c)^2. *Phys. Rev. C* **70**, 015206 (2004).
24. I.A. Qattan *et al.* Precision Rosenbluth measurement of the proton elastic form factors. *Phys. Rev. Lett.* **94**, 142301 (2005).
25. A. Puckett *et al.* Polarization transfer observables in elastic electron proton scattering at $Q^2 = 2.5$, 5.2, 6.8, and 8.5 GeV^2. *Phys. Rev. C* **96**, 055203 (2017).
26. M. Meziane *et al.* Search for effects beyond the Born approximation in polarization transfer observables in $\mathbf{e}p$ elastic scattering. *Phys. Rev. Lett.* **106**, 132501 (2011).
27. J. Arrington, W. Melnitchouk and J.A. Tjon. Global analysis of proton elastic form factor data with two-photon exchange corrections. *Phys. Rev. C* **76**, 035205 (2007).
28. J. Arrington. How well do we know the electromagnetic form factors of the proton? *Phys. Rev. C* **68**, 034325 (2003).
29. G.P. Lepage, S.J. Brodsky. Exclusive processes in perturbative quantum chromodynamics. *Phys. Rev. D* **22**, 2157 (1980).
30. V.L. Chernyak, A.R. Zhitnitskii. Asymptotics of hadronic form factors in QCD. *Yad. Fiz.* **31**, No. 4, 1053 (1980).
31. V.B. Berestetskii, E.M. Lifshitz, L.P. Pitaevskii. *Relativistic Quantum Theory* (Pergamon Press, 1982).

32. L.W. Mo, Y.S. Tsai. Radiative corrections to elastic and inelastic ep and μp scattering. *Rev. Mod. Phys.* **41**, 205 (1969).
33. Y.S. Tsai. Radiative corrections to electron-proton scattering. *Phys. Rev.* **122**, 1898 (1961).
34. A. Afanasev, I. Akushevich, N. Merenkov. Model independent radiative corrections in processes of polarized electron-nucleon elastic scattering. *Phys. Rev. D* **64**, 113009 (2001).
35. A. Afanasev, I. Akushevich, A. Ilyichev, N. Merenkov. QED radiative corrections to asymmetries of elastic ep scattering in hadronic variables. *Phys. Lett. B* **514**, 269 (2001).
36. D. Borisyuk, A. Kobushkin. Radiative corrections to polarization observables in electron-proton scattering. *Phys. Rev. C* **90**, 025209 (2014).
37. S.D. Drell, S. Fubini. Higher electromagnetic corrections to electron-proton scattering. *Phys. Rev.* **113**, 741 (1959).
38. G.K. Greenhut. Two-photon exchange in electron-proton scattering. *Phys. Rev.* **184**, 1860 (1969).
39. A. De Rujula, J.M. Kaplan, E. de Rafael. Elastic scattering of electrons from polarized protons and inelastic electron scattering experiments. *Nucl. Phys. B* **35**, 365 (1971).
40. A. De Rujula, J.M. Kaplan, E. De Rafael. Optimal positivity bounds to the up-down asymmetry in elastic electron-proton scattering. *Nucl. Phys. B* **53**, 545 (1973).
41. B. Pasquini, M. Vanderhaeghen. Resonance estimates for single spin asymmetries in elastic electron-nucleon scattering. *Phys. Rev. C* **70**, 045206 (2004).
42. D. Borisyuk, A. Kobushkin. Target normal spin asymmetry of the elastic ep scattering at resonance energy. *Phys. Rev. C* **72**, 035207 (2005).
43. D. Drechsel, S.S. Kamalov, L. Tiator. Unitary isobar model – MAID2007. *Eur. Phys. J. A* **34**, 69 (2007).
44. A. Afanasev, N.P. Merenkov. Collinear photon exchange in the beam normal polarization asymmetry of elastic electron-proton scattering. *Phys.Lett. B* **599**, 48 (2004).
45. M. Gorchtein. Beam normal spin asymmetry in the quasi-RCS approximation. *Phys. Rev. C* **73**, 055201 (2006).
46. D. Borisyuk, A. Kobushkin. Beam normal spin asymmetry of elastic eN scattering in the leading logarithm approximation. *Phys. Rev. C* **73**, 045210 (2006).
47. P. van Nieuwenhuizen. Muon-electron scattering cross-section to order α^3. *Nucl. Phys. B* **28**, 429 (1971).
48. P.G. Blunden, W. Melnitchouk, J.A. Tjon. Two-photon exchange in elastic electron-nucleon scattering. *Phys. Rev. C* **72**, 034612 (2005).
49. G. 't Hooft, M.J.G. Veltman. Scalar one loop integrals. *Nucl. Phys.* **B153**, 365 (1979).
50. L.C. Maximon, J.A. Tjon. Radiative corrections to electron proton scattering. *Phys. Rev. C* **62**, 054320 (2000).
51. D. Borisyuk, A. Kobushkin. Box diagram in the elastic electron-proton scattering. *Phys. Rev. C* **74**, 065203 (2006).
52. D. Borisyuk, A. Kobushkin. Two-photon exchange in dispersion approach. *Phys. Rev. C* **78**, 025208 (2008).
53. S. Kondratyuk, P.G. Blunden, W. Melnitchouk, J.A. Tjon. Δ resonance contribution to two-photon exchange in electron-proton scattering. *Phys. Rev. Lett.* **95**, 172503 (2005).
54. S. Kondratyuk, P.G. Blunden. Contribution of spin 1/2 and 3/2 resonances to two-photon exchange effects in elastic electron-proton scattering. *Phys. Rev. C* **75**, 038201 (2007).
55. D. Borisyuk, A. Kobushkin, unpublished.
56. D. Borisyuk, A. Kobushkin. On Δ resonance contribution to two-photon exchange amplitude. *Phys. Rev. C* **86**, 055204 (2012).
57. D. Borisyuk, A. Kobushkin. Two-photon-exchange amplitude with πN intermediate states: P_{33} channel. *Phys. Rev. C* **89**, 025204 (2014).
58. D. Borisyuk, A. Kobushkin. Two-photon exchange amplitude with πN intermediate states: Spin-1/2 and spin-3/2 channels. *Phys. Rev. C* **92**, 035204 (2015).
59. M. Tanabashi *et al.* (Particle Data Group). 18. Structure Functions. 18.6. Generalized parton distributions. *Phys. Rev. D* **98**, 030001 (2018).
60. Y.C. Chen, *et al.* Partonic calculation of the two-photon exchange contribution to elastic electron-proton scattering at large momentum transfer. *Phys. Rev. Lett.* **93**, 122301 (2004).
61. A.V. Afanasev *et al.* The two-photon exchange contribution to elastic electron-nucleon scattering at large momentum transfer. *Phys. Rev. D* **72**, 013008 (2005).
62. D. Borisyuk, A. Kobushkin. Perturbative QCD predictions for two-photon exchange. *Phys. Rev. D* **79**, 034001 (2009).
63. N. Kivel, M. Vanderhaeghen. Two-photon exchange in elastic electron-proton scattering: QCD factorization approach. *Phys. Rev. Lett.* **103**, 092004 (2009).
64. N. Kivel, M. Vanderhaeghen. Two-photon exchange corrections to elastic electron-proton scattering at large momentum transfer within the SCET approach. *JHEP* **1304**, 029 (2013).
65. I. Sick. On the RMS radius of the proton. *Phys. Lett. B* **576**, 62 (2003).
66. W.A. McKinley, H. Feshbach. The Coulomb scattering of relativistic electrons by nuclei. *Phys. Rev.* **74**, 1759 (1948).
67. R.H. Dalitz. On higher Born approximations in potential scattering. *Proc. Roy. Soc. Lond.* **206**, 509 (1951).
68. R. Rosenfelder. Coulomb corrections to elastic electron-proton scattering and the proton charge radius. *Phys. Lett. B* **479**, 381 (2000).

69. R.R. Lewis, jr. Potential scattering of high-energy electrons in second Born approximation. *Phys. Rev.* **102**, 537 (1956).
70. D. Borisyuk, A. Kobushkin. Two-photon exchange at low Q^2. *Phys. Rev. C* **75**, 038202 (2007).
71. D. Borisyuk, A. Kobushkin. Two-photon exchange in non-relativistic approximation. *arXiv:1811.06928*.
72. P.G. Blunden, I. Sick. Proton radii and two-photon exchange. *Phys. Rev. C* **72**, 057601 (2005).
73. D. Borisyuk. Proton charge and magnetic rms radii from the elastic ep scattering data. *Nucl. Phys. A* **843**, 59 (2010).
74. P.J. Mohr, B.N. Taylor, D.B. Newell. CODATA recommended values of the fundamental physical constants: 2010. *Rev. Mod. Phys.* **84**, 1527 (2012).
75. R. Gilman *et al.* Studying the Proton "Radius" Puzzle with μp Elastic Scattering. *arXiv:1303.2160*.
76. J.C. Bernauer *et al.* High-precision determination of the electric and magnetic form factors of the proton. *Phys. Rev. Lett.* **105**, 242001 (2010).
77. J.C. Bernauer *et al.* Electric and magnetic form factors of the proton. *Phys. Rev. C* **90**, 015206 (2014).
78. I.A. Rachek *et al.* Measurement of the two-photon exchange contribution to the elastic $e \pm p$ scattering cross-sections at the VEPP-3 storage ring. *Phys. Rev. Lett.* **114**, 062005 (2015).
79. D. Adikaram *et al.* Towards a resolution of the proton form factor problem: new electron and positron scattering data. *Phys. Rev. Lett.* **114**, 062003 (2015).
80. B.S. Henderson. Results from the OLYMPUS experiment on the contribution of hard two-photon exchange to elastic electron-proton scattering. *PoS* **310**, 149 (2018).
81. J. Arrington. Extraction of two-photon contributions to the proton form-factors. *Phys. Rev. C* **71**, 015202 (2005).
82. D. Borisyuk, A. Kobushkin. Phenomenological analysis of two-photon exchange effects in proton form factor measurements. *Phys. Rev. C* **76**, 022201 (2007).
83. D. Borisyuk, A. Kobushkin. Two-photon exchange amplitudes for the elastic ep scattering at $Q^2 = 2.5$ GeV^2 from the experimental data. *Phys. Rev. D* **83**, 057501 (2011).
84. J. Guttmann, N. Kivel, M. Meziane, M. Vanderhaeghen. Determination of two-photon exchange amplitudes from elastic electron-proton scattering data. *Eur. Phys. J. A* **47**, 77 (2011).
85. A. Afanasev, A. Aleksejevs, S. Barkanova. Two photon exchange for exclusive pion electroproduction. *Phys. Rev. D* **88**, 053008 (2013).
86. S. Kondratyuk, P.G. Blunden. Calculation of two-photon exchange effects for Delta production in electron-proton collisions. *Nucl. Phys. A* **778**, 44 (2006).
87. J.A. Tjon, P.G. Blunden, W. Melnitchouk. Detailed analysis of two-boson exchange in parity-violating e-p scattering. *Phys. Rev. C* **79**, 055201 (2009).
88. A. Afanasev, M. Strikman, C. Weiss. Transverse target spin asymmetry in inclusive DIS with two-photon exchange. *Phys. Rev. D* **77**, 014028 (2008).
89. Dian-Yong Chen, Yu-Bing Dong. Two-photon exchange in the $\ell + p \to \ell + p$ process with a massive lepton. *Phys. Rev. C* **87**, 045209 (2013).
90. O. Tomalak, M. Vanderhaeghen. Two-photon exchange corrections in elastic muon-proton scattering. *Phys. Rev. D* **90**, 013006 (2014).
91. O. Koshchii, A. Afanasev. Contribution of σ-meson exchange to elastic lepton-proton scattering. *Phys. Rev. D* **94**, 116007 (2016).
92. D. Borisyuk. Meson exchange in lepton-nucleon scattering and the proton radius puzzle. *Phys. Rev. C* **96**, 055201 (2017).
93. O. Tomalak, M. Vanderhaeghen. Subtracted dispersion relation formalism for the two-photon exchange correction to elastic electron-proton scattering: Comparison with data. *Eur. Phys. J. A* **51**, 24 (2015).
94. O. Tomalak, M. Vanderhaeghen. Dispersion relation formalism for the two-photon exchange correction to elastic muon-proton scattering: Elastic intermediate state. *Eur. Phys. J. C* **78**, 514 (2018).
95. Hong-Yu Chen, Hai-Qing Zhou. Meson exchange effects in elastic ep scattering at loop level and the electromagnetic form factors of the proton. *Phys. Rev. C* **90**, 045205 (2014).
96. Yu Bing Dong, D.Y. Chen. Two-photon exchange effect on deuteron electromagnetic form factors. *Phys. Lett. B* **675**, 426 (2009).
97. Yu Bing Dong. Estimate of the two-photon exchange effect on deuteron electromagnetic form factors. *Phys. Rev. C* **80**, 025208 (2009).
98. A.P. Kobushkin, Ya.D. Krivenko-Emetov, S. Dubnicka. Elastic electron-deuteron scattering beyond one-photon exchange. *Phys. Rev. C* **81**, 054001 (2010).
99. A.P. Kobushkin, Ya.D. Krivenko-Emetov, S. Dubnicka, A.Z. Dubnickova. Two-photon exchange and elastic scattering of longitudinally polarized electron on polarized deuteron. *Phys. Rev. C* **84**, 054007 (2011).
100. Dian-Yong Chen, Yu-Bing Dong. Two-photon exchange corrections to single spin asymmetry of neutron and He-3. *Commun. Theor. Phys.* **55**, 489 (2011).
101. A.P. Kobushkin, Ju. V. Timoshenko. Two-photon exchange in electron-trinucleon elastic scattering. *Phys. Rev. C* **88**, 044002 (2013).
102. P.G. Blunden, W. Melnitchouk, J.A. Tjon. Two-photon exchange corrections to the pion form factor. *Phys. Rev. C* **81**, 018202 (2010).
103. Yu-Bing Dong, S.D. Wang. Effect of two-photon exchange on the charged pion form factor. *Phys. Lett. B* **684**, 123 (2010).
104. Hai Qing Zhou. Gauge Invariant two-photon-exchange contributions in $e^- \pi^+ \to e^- \pi^+$. *Phys. Lett. B* **706**, 82 (2011).

105. D. Borisyuk, A. Kobushkin. Two-photon exchange in elastic electron-pion scattering. *Phys. Rev. C* **83**, 025203 (2011).

Received 09.12.19

Д. Борисюк, А. Кобушкін

ДВОФОТОННИЙ ОБМІН
У ПРУЖНОМУ РОЗСІЯННІ
ЕЛЕКТРОНІВ НА АДРОННИХ СИСТЕМАХ

Дається огляд різних аспектів двофотонного обміну (ДФО) у пружному розсіянні електронів на протонах, як при низьких, так і при високих Q^2. Уявна частина амплітуди ДФО приводить до появи одночастинкових спінових асиметрій. Розглянуто різні підходи до розрахунку цих спостережуваних. Дійсна частина амплітуди ДФО впливає на переріз розсіяння неполяризованих частинок і подвійні спінові спостережувані, та, найбільш імовірно, призводить до розбіжності двох методів вимірювання формфакторів протона. Обговорюються методи розрахунку амплітуд ДФО, зокрема "адронний" та "кварк-глюонний" підходи, дисперсійний метод, що може використовуватися при низьких та середніх Q^2, а також зв'язок з проблемою радіуса протона. Розглянуто сучасний стан експериментів із прямого спостереження ефектів ДФО за допомогою вимірювання зарядової асиметрії пружного розсіяння, та спроби визначення амплітуд ДФО, виходячи з експериментальних даних. Також наводиться огляд двофотонних ефектів у інших процесах, таких як розсіяння мюонів на протонах, електронів на ядрах, на піонах та інші.

Ключові слова: двофотонний обмін, пружне розсіяння, формфактор протона.